INORGANIC CHEMISTRY
FRONTIERS

PAPER

Cite this: *Inorg. Chem. Front.*, 2014, **1**, 83

$[NH_2NH_3][M(HCOO)_3]$ (M = Mn^{2+}, Zn^{2+}, Co^{2+} and Mg^{2+}): structural phase transitions, prominent dielectric anomalies and negative thermal expansion, and magnetic ordering†

Sa Chen, Ran Shang, Ke-Li Hu, Zhe-Ming Wang* and Song Gao*

Received 5th September 2013,
Accepted 14th November 2013

DOI: 10.1039/c3qi00034f

rsc.li/frontiers-inorganic

We report here a new class of ammonium metal–formate frameworks of $[NH_2NH_3][M(HCOO)_3]$ (M = Mn^{2+}, Zn^{2+}, Co^{2+} and Mg^{2+}) incorporating hydrazinium as the cationic template and component. The perovskite Mn and Zn members possess anionic $4^{12}\cdot6^3$ metal–formate frameworks with cubic cavities occupied by the $NH_2NH_3^+$ cations, while the Co and Mg members have chiral $4^9\cdot6^6$ metal–formate frameworks, with chiral hexagonal channels accommodating $NH_2NH_3^+$ cations. On heating, the Mn and Zn members undergo phase transitions around 350 K. The structures change from low temperature (LT) polar phases in $Pna2_1$ to high temperature (HT) non-polar phases in *Pnma*, due to the thermally activated librational movement of the NH_2 end of the $NH_2NH_3^+$ in the cavity and significant framework regulation. The Co and Mg members in LT belong to non-polar $P2_12_12_1$, are probably antiferroelectric, and they show phase transitions at 380 K (Co) and 348 K (Mg), and the structures change to polar HT phases in $P6_3$, triggered by the order–disorder transition of the cation from one unique orientation in LT to three of trigonally-disorder state in HT. Accompanying the phase transitions, which are ferro- to para-electric for Mn and Zn members while antiferro- to ferro-electric for Co and Mg, prominent anisotropic thermal expansions including negative ones, and dielectric anomalies, are observed. The spontaneous polarization values are estimated at 3.58 (Mn, 110 K), 3.48 (Zn, 110 K), 2.61 (Co, 405 K) and 3.44 (Mg, 400 K) μC cm^{-2}, respectively, based on the positive and negative charge separations in the polar structures. The structure–property relevance is established based on the order–disorder transitions of $NH_2NH_3^+$ and the conformity and adaptability of the metal–formate frameworks to match such order–disorder alternations. The Mn and Co members show spin-canted antiferromagnetic long-range-ordering, with Néel temperatures of 7.9 K and 13.9 K, respectively. Therefore, the two members show coexistence of electric and magnetic orderings in the low temperature region, and they are possible molecule-based multiferroics.

Introduction

In pursuit of new devices and advanced materials, it is more and more desirable to combine or integrate different properties and functionalities within one single phase material. The renaissance of multiferroics in the last decade represents such trend.[1,2] Multiferroics are of great importance for both fundamental science and the potential applications in new devices based on the mutual controls of magnetic and electric fields. The materials of metal–organic frameworks, MOFs, have received considerable attention for multi-functional materials.[3–7] These materials, by combining inorganic and organic components, can not only possess new and interesting properties or functionalities,[4] originating from their organic–inorganic hybrid character,[3] but also afford possible coexistence and/or synergism of multiple functionalities within one material. Indeed, multi-functionalities such as conductivity and magnetism,[5] magnetic and optical properties,[6] porosity and magnetism,[7] have been all realized in MOF materials, by incorporating suitable inorganic and organic building blocks and structural features within MOFs. More recently, several MOFs showing coexistence of magnetic and electric orderings or multiferroics have emerged,[8] however, these MOF-/molecule-based multiferroics are still very limited compared to the much more well developed pure inorganic ones.[1,2] On the other hand, it has been now realized that MOFs themselves

Beijing National Laboratory for Molecular Sciences, State Key Laboratory of Rare Earth Materials Chemistry and Applications, College of Chemistry and Molecular Engineering, Peking University, Beijing 100871, PR China. E-mail: zmw@pku.edu.cn, gaosong@pku.edu.cn; Fax: +86-10-62751708

† Electronic supplementary information (ESI) available: Tables S1 to S4, Fig. S1 to S13, CIF files. CCDC 958452–958467. For ESI and crystallographic data in CIF or other electronic format see DOI: 10.1039/c3qi00034f

could display a rich variety of physical properties and critical phenomena or phase transitions.[9] In addition to the magnetic[10] and electric[11,12] transitions, the unusual mechanical properties of negative thermal expansion (NTE)[13–16] and the related framework dynamics,[17] negative linear compressibility (NLC),[18] pressure or temperature induced amorphization[19] and so on have aroused great interest from both a fundamental and a practical point of view, as have those for conventional materials such as oxides.[9] These properties are all very closely linked to the structural modifications and/or structural transitions, therefore are possibly also linked one to another. The close link between anisotropic thermal expansion (ATE), including NTE, and the ferro- to para-electric transition is well known for classical ferroelectrics such as $BaTiO_3$ (BTO) and potassium dihydrogen phosphate (KDP) in which the underlying mechanism is order–disorder transitions of cationic components.[20]

Along these lines, we and other authors have studied the ammonium metal–formate frameworks (hereafter abbr. AMFFs) systematically.[21] AMFFs are promising MOFs for magnetic and/or electric orderings and phase transitions because of the following observations. (i) The formate $HCOO^-$, the smallest and simplest carboxylate, can adopt various bridging modes such as *syn–syn*, *anti–anti*, *syn–syn*/*anti*, all short bridges, to link metal ions, and it has small stereo effects. These are all beneficial properties for the formation of MOFs, and for the significant magnetic coupling between magnetic metal sites. (ii) Formate is a good hydrogen-bonding acceptor (hereafter HB = hydrogen-bonding/bond), and the ammonium ions are good HB donors. The combination of such components could produce HB systems required for ferro-/antiferro-electric properties in molecule-based materials, such as those in traditional KDP and TGS,[20] and recently organic ones.[22] (iii) The metal–formate frameworks have shown malleability and adaptability to conform to the ammonium ions employed, not only the different framework structure types depending on the size, shape, charge *etc.* of the ammonium ions, but also the framework flexibility and modulation to the order/disorder status of the cations. For AMFFs, many interesting results and developments have been recently reported.[21,22–34] The $[NH_4][M(HCOO)_3]$[23] and $[(CH_3)_2NH_2][M(HCOO)_3]$[24–26] series (M = 3d magnetic metal), known as MOF-based multiferroics, display coexistence or synergism of magnetic and electric orderings. Giant dielectric anomalies and relaxor behaviors have been observed for $[(CH_2)_3NH_2][M(HCOO)_3]$.[27] In several lanthanide metal systems, magnetic relaxation behaviors and structural transitions have been observed.[28] $[C(NH_2)_3][Cu/Cr(HCOO)_3]$ have been suggested by DFT calculations to show possible magnetoelectric effect, but this is still awaiting experimental confirmation.[29] NTE and NLC have been observed for $[NH_4][M(HCOO)_3]$[23] and $[CH_3NH_3][Mn(HCOO)_3]$.[24a] Para- to antiferro-electric transitions of unusual structural alternations together with Néel N-type ferrimagnetism have been observed in mixed-valence $[(CH_3)_2NH_2][Fe^{III}Fe^{II}(HCOO)_6]$.[30] It has been noted that the order–disorder transitions of ammonium cations could occur in most of these AMFFs,[22–34] as observed in many other systems including ammonium components.[35–38]

To build upon these interesting results and to continue our studies[21,23–25,27,28,29a,33,34] on AMFFs, in this work we use the hydrazinium, $NH_2NH_3^+$, as the cationic component and template to construct a new AMFF class of $[NH_2NH_3][M(HCOO)_3]$, in which the four compounds are named as **1Mn**, **2Zn**, **3Co** and **4Mg** for M = Mn^{2+}, Zn^{2+}, Co^{2+} and Mg^{2+}, respectively. The $NH_2NH_3^+$ has an intermediate size, larger than NH_4^+ and $HONH_3^+$ ions[23,33] but smaller than $CH_3NH_3^+$ and other larger mono-ammonium ions,[24–27,29–32] and it is a good HB donor and possible acceptor. The middle size of hydrazinium resulted in two typical AMFF structures within the series, one is the perovskites (**1Mn** and **2Zn**) and the other the chiral frameworks (**3Co** and **4Mg**). The materials all displayed interesting structural phase transitions with critical temperatures (T_C values) close to or above 350 K, comparable to inorganic BTO, accompanied by significant dielectric anomalies and ATE/NTE due to the order–disorder transitions of hydrazinium and the framework modulations. The materials were characterized by thermal analyses, variable temperature (VT) single crystal X-ray diffraction (SXRD) and powder X-ray diffraction (PXRD), and dielectric measurements. The magnetic **1Mn** and **3Co** showed long-range-ordering (LRO) of spin-canted antiferromagnetism (AF) in the low temperature region.

Experimental section

Synthesis

All chemicals were commercially available, reagent grade, and used without further purification. Cautionary note: perchlorate compounds are potentially explosive. They should be prepared in small quantities and handled with care.

The four compounds were synthesized by mild solution methods. Typically, **1Mn** was prepared as follows. 5.0 ml of methanol solution containing formic acid 3.94 g (80 mmol) and an aqueous solution of 85% hydrazine 0.35 g (6.0 mmol) were mixed with 5.0 ml of methanol solution containing $Mn(ClO_4)_2{\cdot}6H_2O$ 0.36 g (1.0 mmol). The mixed solution was kept undisturbed. After two days, the block-shaped colorless crystals of X-ray quality were collected, washed with ethanol and air-dried. The yield is 86% based on $Mn(ClO_4)_2{\cdot}6H_2O$. **2Zn**, **3Co** and **4Mg** were obtained similarly with yields of 80%, 96% and 90% for **2Zn**, **3Co** and **4Mg**, respectively. Anal. (%) **1Mn**, calcd for $C_3H_8MnN_2O_6$: C, 16.15; H, 3.61; N, 12.56; found: C, 16.15; H, 3.52; N, 12.53; **2Zn**, calcd for $C_3H_8ZnN_2O_6$: C, 15.43; H, 3.45; N, 12.00; found: C, 15.48; H, 3.34; N, 11.89; **3Co**, calcd for $C_3H_8CoN_2O_6$: C, 15.87; H, 3.55; N, 12.34; found: C, 15.99; H, 3.51; N, 12.21; **4Mg**, calcd for $C_3H_8MgN_2O_6$: C, 18.73; H, 4.19; N, 14.56; found: C, 18.68; H, 4.16; N, 14.61. The crystals of **1Mn** and **2Zn** are nearly rectangular blocks or thick plates, while the crystals of **3Co** and **4Mg** are hexagonal blocks or pyramids (Fig. S1†).

X-ray crystallography and physical measurements

The SXRD intensity data for the single crystals of the four compounds at low temperatures (LT) were collected on a Nonius Kappa CCD diffractometer (CCD-1),[39] and data at high temperatures (HT) on an Agilent Technology SuperNova Dual Atlas CCD diffractometer (CCD-2),[40] using monochromated Mo Kα radiation (λ = 0.71073 Å) and equipped temperature control systems. Crystals showed reversible phase transitions and all kept good crystallinity, though single crystals of **3Co** and **4Mg** became twinned from HT back to LT. All structures were solved by direct method and refined by full-matrix least-squares on F^2 using SHELX program.[41] The H atoms were located from the difference Fourier synthesis, but constrained according to the ideal geometries in refinements. For **3Co** and **4Mg**, the HT structures were solved in space groups $P6_3$ and $P6_322$. However, the structures refined in $P6_3$ resulted in significantly lower R factors (for **3Co**, R_1 = 0.016 in $P6_3$ while 0.021 in $P6_322$) and better models for the trigonally disordered hydrazinium with rational molecular geometry. The crystallographic data are briefly summarized in Table 1 while the details are reported in Table S1,† and the selected molecular geometries are listed in Table S2† (**1Mn** and **2Zn**) and Table S3† (**3Co** and **4Mg**). CCDC-958452 to 958467 contain the supplementary crystallographic data for this paper.

PXRD data were collected in the range of 5° < 2θ < 60° at room temperature (RT) for the bulk samples and the pressed tablet samples on a Rigaku Dmax 2000 diffractometer, and VT PXRD patterns for the pressed tablet samples were collected on CCD-2, using Cu Kα radiation.

Elemental analysis of C/H/N was performed on an Elementar Vario MICRO CUBE analyzer. FTIR spectra in the range of 4000 to 600 cm^{-1} were recorded for pure samples on a NICOLET iN10 MX spectrometer. Thermal analyses were performed on a TA SDT Q600 simultaneous DSC-TGA instrument at the rate of 5 °C min^{-1} in air flow. The DSC measurements were performed on a TA Q100 DSC analyzer at the rate of 5 °C min^{-1} in N_2 flow and cycled two or three times.

The temperature-dependent ac (alternate current) dielectric permittivity measurements were carried out on a TH2828 Precision LCR meter under 20 frequencies from 100 Hz to 1 MHz and an applied voltage of 1.0 V, at a temperature sweeping rate of *ca.* 1 K min^{-1} in dried N_2 flow. Samples were ground and pressed into tablets under a pressure of *ca.* 2 GPa. The phase purity of the pressed tablets and the absence of pressure-induced phase transitions were confirmed by PXRD (Fig. S2†). The capacitors were made by painting the two faces of the tablet pieces with silver conducting paste and copper or golden wires as the electrodes. These capacitors were kept vacuum-dried over silica gel for more than two weeks and finally coated by a very thin layer of AB glue or vaseline before the dielectric measurements, in order to avoid the influence of moisture. The area and thickness of the capacitors were measured under a microscope with a Phenix CCD eye and the software.

Magnetic measurements for **1Mn** and **3Co** were performed on a Quantum Design MPMSXL5 SQUID system with polycrystalline samples tightly packed and sealed in a capsule. Diamagnetic corrections were estimated using Pascal constants (-91×10^{-6} and -89×10^{-6} cm^3 mol^{-1} for **1Mn** and **3Co**, respectively)[42] and background correction by experimental measurement on sample holders.

Results and discussion

Synthesis, IR spectra, thermal properties, and structural phase transitions

The four AMFF materials were prepared under ambient conditions by employing suitable metal perchlorate salts, hydrazine (85% aqueous solution) and formic acid in methanol (see above). This mild solution chemistry method has proved to be very successful, general, convenient and performed easily in the preparation of various AMFFs in the last few years by us,[21,23,24,27–29,33,34] though sometimes solvothermal methods were employed.[25,26,30,32] The PXRD patterns (Fig. S2†) confirmed the phase purity of the products, so the small water component of the commercial aqueous hydrazine (85%) did not produce impurities of metal–formate dihydrate in the products, as frequently encountered.[21] Similar observations were reported for the preparation of the mixed metal perovskites $[CH_3NH_3][Mn_xZn_{1-x}(HCOO)_3]$,[24b] niccolite $[CH_3NH_2CH_2CH_2NH_2CH_3][Zn_2(HCOO)_6]$,[34b] and the perovskite series of $[C(NH_2)_3][M(HCOO)_3]$.[29a] Another interesting observation for the present series is that **1Mn** and **2Zn** possess the most popular perovskite AMFF structures among several $[AmineH][M(HCOO)_3]$ series for mono ammonium ions[24–27,29,31,32] where $AmineH^+$ = $CH_3NH_3^+$, $(CH_3)_2NH_2^+$, $CH_3CH_2NH_3^+$, $(CH_2)_3NH_2^+$, $C(NH_2)_3^+$ and $(NH_2)_2CH^+$, while **3Co** and **4Mg** belong to the chiral structures of the type $[NH_4][M(HCOO)_3]$[23] and the recently reported $[HONH_3][M(HCOO)_3]$[33] series. Given the fact that the four compounds have the same constituents except the different metal ions, and usually within one AMFF series the Mn, Fe, Co, Ni, Zn and Mg members are isostructural,[21] this observation is quite unexpected. For each metal ion we could expect the existence of two phases or polymorphs. Indeed, we have found that for the Fe member the product is a mixture of two such phases.[43] We are still trying to obtain the two Fe phases in pure form so that they will be reported in the future, as well as to prepare the perovskite phases of **3Co** and **4Mg** and the chiral phases of **1Mn** and **2Zn**. Finally, attempts to prepare the Ni and Cu members within this series were not successful, probably due to the very low solubility of the Ni member[21] and the easy reduction of Cu^{2+} by hydrazine.

The IR spectra of the four compounds are quite similar but still show some slight differences (Fig. S3†), given the fact that the structures belong to two types. The IR absorption bands and their assignments are given in Table S4,† and they are characteristic of $NH_2NH_3^+$ and $HCOO^-$.[33,44]

The combined TGA-DSC runs up to 800 °C are shown in Fig. S4.† These materials basically showed two weight loss procedures on their TGA traces. The first endothermic one

Table 1 Summary of crystallographic data for **1Mn**, **2Zn**, **3Co** and **4Mg**

1Mn, formula = $C_3H_8MnN_2O_6$, fw = 223.05				
T (K)	110	200	290	400
Crystal system	Orthorhombic	Orthorhombic	Orthorhombic	Orthorhombic
Space group	$Pna2_1$	$Pna2_1$	$Pna2_1$	$Pnma$
a (Å)	8.9319(3)	8.9503(3)	8.9448(3)	8.8505(3)
b (Å)	7.8190(2)	7.8214(2)	7.8403(3)	11.8785(4)
c (Å)	11.6928(5)	11.7189(5)	11.7669(5)	7.9240(3)
α (°)	90	90	90	90
β (°)	90	90	90	90
γ (°)	90	90	90	90
V (Å^3)	816.61(5)	820.37(5)	825.21(5)	833.06(5)
Z, D_c (g cm^{-3})	4, 1.814	4, 1.806	4, 1.795	4, 1.778
μ (Mo K_α) (mm^{-1}), F(000)	1.613, 452	1.606, 452	1.597, 452	1.581, 452
No. total/uniq./obs. reflns.	15 236/2093/1540	15 362/2101/1439	15 111/2113/1378	12 844/1077/873
R_1, wR_2 (for $I \geq 2\sigma(I)$)	0.0248, 0.0435	0.0243, 0.0408	0.0259, 0.0426	0.0297, 0.0779
GOF	0.912	0.885	0.885	1.226
2Zn, formula = $C_3H_8ZnN_2O_6$, fw = 233.48				
T (K)	110	200	290	375
Crystal system	Orthorhombic	Orthorhombic	Orthorhombic	Orthorhombic
Space group	$Pna2_1$	$Pna2_1$	$Pna2_1$	$Pnma$
a (Å)	8.6640(3)	8.6806(3)	8.6748(3)	8.5958(3)
b (Å)	7.7157(2)	7.7235(3)	7.7488(3)	11.6442(5)
c (Å)	11.4824(4)	11.5056(3)	11.5478(4)	7.8468(3)
α (°)	90	90	90	90
β (°)	90	90	90	90
γ (°)	90	90	90	90
V (Å^3)	767.58(4)	771.39(4)	776.23(5)	785.40(5)
Z, D_c (g cm^{-3})	4, 2.020	4, 2.010	4, 1.998	4, 1.975
μ (Mo K_α) (mm^{-1}), F(000)	3.196, 472	3.181, 472	3.161, 472	3.124, 472
No. total/uniq./obs. reflns.	14 003/1944/1427	14 258/1965/1369	14 396/1988/1329	11 343/1024/756
R_1, wR_2 (for $I \geq 2\sigma(I)$)	0.0230, 0.0426	0.0227, 0.0402	0.0233, 0.0395	0.0294, 0.0727
GOF	0.931	0.942	0.892	1.154
3Co, formula = $C_3H_8CoN_2O_6$, fw = 227.04				
T (K)	110	200	290	405
Crystal system	Orthorhombic	Orthorhombic	Orthorhombic	Hexagonal
Space group	$P2_12_12_1$	$P2_12_12_1$	$P2_12_12_1$	$P6_3$
a (Å)	7.9435(2)	7.9415(2)	7.9341(3)	7.9157(3)
b (Å)	13.8339(4)	13.8460(5)	13.8697(7)	7.9157(3)
c (Å)	7.3016(2)	7.3103(2)	7.3361(3)	7.4836(3)
α (°)	90	90	90	90
β (°)	90	90	90	90
γ (°)	90	90	90	120.00
V (Å^3)	802.37(4)	803.83(4)	807.29(6)	406.09(3)
Z, D_c (g cm^{-3})	4, 1.880	4, 1.876	4, 1.868	2, 1.857
μ (Mo K_α) (mm^{-1}), F(000)	2.136, 460	2.132, 460	2.123, 460	2.110, 230
No. total/uniq./obs. reflns.	16 158/2071/1771	16 313/2074/1711	14 202/2077/1607	6226/672/648
R_1, wR_2 (for $I \geq 2\sigma(I)$)	0.0244, 0.0458	0.0263, 0.0490	0.0279, 0.0497	0.0157, 0.0422
GOF	0.988	0.965	0.955	1.118
4Mg, formula = $C_3H_8MgN_2O_6$, fw = 192.42				
T (K)	110	200	292	400
Crystal system	Orthorhombic	Orthorhombic	Orthorhombic	Hexagonal
Space group	$P2_12_12_1$	$P2_12_12_1$	$P2_12_12_1$	$P6_3$
a (Å)	7.8999(2)	7.8928(2)	7.8888(2)	7.8798(3)
b (Å)	13.7505(4)	13.7693(4)	13.7799(4)	7.8798(3)
c (Å)	7.3829(2)	7.4007(2)	7.4295(2)	7.5682(4)
α (°)	90	90	90	90
β (°)	90	90	90	90
γ (°)	90	90	90	120.00
V (Å^3)	801.99(4)	804.30(4)	807.64(4)	406.96(3)
Z, D_c (g cm^{-3})	4, 1.594	4, 1.589	4, 1.583	2, 1.570
μ (Mo K_α) (mm^{-1}), F(000)	0.219, 400	0.218, 400	0.217, 400	0.216, 200
No. total/uniq./obs. reflns.	14 126/1993/1864	14 119/1993/1827	14 178/1996/1756	6712/678/654
R_1, wR_2 (for $I \geq 2\sigma(I)$)	0.0249, 0.0652	0.0283, 0.0747	0.0307, 0.0808	0.0260, 0.0698
GOF	1.141	1.099	1.052	1.117

Table 2 Summary of phase transitions and thermal and dielectric properties for **1Mn**, **2Zn**, **3Co** and **4Mg**

Compound	**1Mn**	**2Zn**	**3Co**	**4Mg**
Thermal properties and phase transitions (up = heating, down = cooling, and av = averaged)				
T_C (K), by DSC peaks	357^{up}, 353^{down} 355^{av}	350^{up}, 349^{down} 350^{av}	382^{up}, 377^{down} 380^{av}	349^{up}, 348^{down} 348^{av}
ΔH (kJ mol^{-1}), by DSC	3.9	3.4	3.1	2.6
ΔS (J mol^{-1} K^{-1}), N, by DSC,	10.8, 3.7	9.7, 3.2	8.2, 2.7	7.5, 2.5
T_C (K), by TGA-DSC	357^{up}	352^{up}	381^{up}	350^{up}
T_d (K), by TGA-DSC	400	380	430	450
T_C range (K), by VT PXRD	$350–360^{up}$	$350–360^{up}$	$380–390^{up}$	$340–350^{up}$
T_d (K), by VT PXRD	400	360	410	440
Dielectric properties (from ε' data at 1 MHz)				
$\varepsilon'_{290\ K}$	7.1	8.4	8.4	8.1
T_{turn} [a] (K), and ε' value at turning point in ε'	353, 10.4	342, 12.2	378, 12.6	336, 9.9
T_{peak} or T_{sh}, K, and ε' value at peak or shoulder point in ε'	364peak, 28.0	362sh, 25.4	405sh, 32.1	343sh, 11.2 375sh, 24.1
$T_{d\varepsilon'/dT\ peak}$ (K) at $d\varepsilon'/dT$ peak	362	357	390	340, 364, 415
C and T_0 (K)	HT: 3.2×10^2, 353 LT: 1.4×10^2, 368	LT: 3.3×10^2, 372	LT: 3.3×10^2, 405	I: 3.4×10^3, 508 II: 5.4×10^2, 393
Transition type, LT to HT	Ferro to para	Ferro to para	Antiferro to ferro	Antiferro to ferro
E_a (eV), τ_0 (s), for relaxation				1.03, 1.45×10^{-17}
Estimated P_S [b] (μC cm^{-2})	3.58	3.48	2.61	3.44
Aizu notation	*mmmFmm*2	*mmmFmm*2		

[a] The first turning points from room temperature in ε' *vs.* T plots. [b] Spontaneous polarization.

occurred around 130, 110, 160 and 180 °C (decomposition temperatures T_d = 400, 380, 430 and 450 K, Table 2) for **1Mn**, **2Zn**, **3Co** and **4Mg**, respectively, and the weight losses were 33.4 (**1Mn**), 33.3 (**2Zn**), 33.8 (**3Co**) and 40.5% (**4Mg**), corresponding to the departure of one NH_2NH_2·HCOOH per formula with calculated weight losses of 33.5 (**1Mn**), 33.4 (**2Zn**), 34.4 (**3Co**) and 40.6% (**4Mg**), respectively, although for **1Mn**, **2Zn** and **3Co** this procedure might include two sub-steps. The energy acquirements were 120 kJ mol^{-1}. After the first decomposition, **1Mn** and **3Co** further decomposed around 300 °C with high exothermic peaks and energy releases of 540 (**1Mn**) and 690 (**3Co**) kJ mol^{-1}. **2Zn** further decomposed in two steps, one weak endothermic (3 kJ mol^{-1}) around 400 °C and one strong exothermic (290 kJ mol^{-1}) around 580 °C. The pyrolysis of **4Mg** occurred at *ca.* 420 °C with an energy release of 57 kJ mol^{-1}. The final residues were 35.7, 31.7, 33.8 and 20.8% for **1Mn**, **2Zn**, **3Co** and **4Mg**, respectively, in agreement with the calculated values of 35.4, 33.0, 34.9 and 20.9% based on Mn_2O_3, ZnO, CoO and MgO. The thermal stabilities of the present series are similar to other mono-ammonium metal–formate series[23–25,33] except for the most stable $[C(NH_2)_3]$-$[M(HCOO)_3]$ structures.[29a] It should be noted that the four materials showed small but perceivable endothermic peaks around 84, 79, 108 and 77 °C (357, 352, 381 and 350 K) for **1Mn**, **2Zn**, **3Co** and **4Mg**, respectively, before their first decomposition in the DSC plots (Fig. S4b,† inset), and these indicated the occurrence of phase transitions.

These phase transitions were further confirmed by the more accurate DSC measurements (Fig. 1, Fig. S5,† Table 2). In the DSC traces endo/exothermic peaks were clearly observed at 357/353 K (**1Mn**), 350/349 K (**2Zn**), 382/377 K (**3Co**) and 349/347 K (**4Mg**, the highest peak positions), respectively, on heating/cooling, showing thermal hysteresis of few Kelvin. The

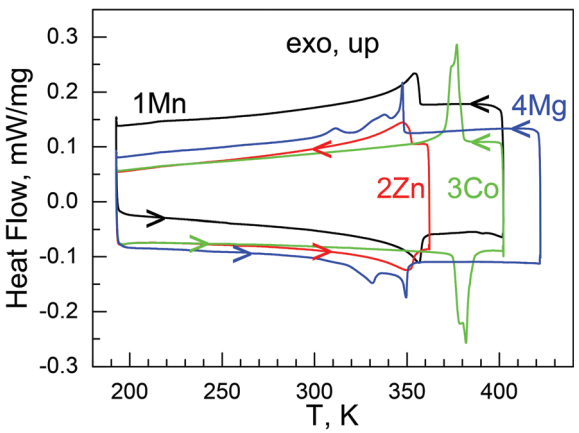

Fig. 1 The DSC traces for the four compounds, all first cycle.

T_C values could be defined to be the averaged values, 355 K (**1Mn**), 350 K (**2Zn**), 380 K (**3Co**), and 348 K (**4Mg**). **1Mn** and **2Zn** displayed single, cycle-independent peaks with a somewhat extending tail on the low temperature side. **3Co** possessed narrow and more prominent peaks, showing a shoulder in the first cycle. In the second cycle, the shoulder disappeared on heating but restored on the followed cooling. **4Mg** behaved in a quite complicated manner, with two, even three thermic peaks in the range of 330 to 350 K, indicating a probably multi-step phase transition. The ΔH values (in kJ mol^{-1}) for the phase transitions were estimated at 3.9 ± 0.2 (**1Mn**), 3.4 ± 0.1 (**2Zn**), 3.1 ± 0.1 (**3Co**), 2.6 ± 0.1 (**4Mg**), and the ΔS ($\Delta S = \Delta H/T_C$)[45] values were estimated at 10.8 to 7.5 J mol^{-1} K^{-1} for the phase transitions. From the Boltzmann equation, $\Delta S = R \ln(N)$, R being the gas constant and N the ratio of the numbers of respective distinguishable states of different phases,

N values of 3.7 to 2.5 could be calculated (Table 2). These values are roughly agreeable with 2 or 3 discrete states for the disordered $NH_2NH_3^+$ cation in the HT phases but 1 for the ordered $NH_2NH_3^+$ cation in the LT phases (see below). It is noted that the materials of the present series have high T_C values, all close to the typical ferroelectric oxide BTO,[20] comparing with the previously reported AMFF series showing structural phase transitions, $[(CH_3)_2NH_2][M(HCOO)_3]$,[26,31] $[NH_4][M(HCOO)_3]$[23] and $[(CH_2)_3NH_2][M(HCOO)_3]$,[27] with T_C values below room temperature.

The VT PXRD patterns for the four compounds are shown in Fig. S6.† On heating, the phase transitions were evidenced by the changes, highlighted by stars in the patterns occurring around the individual T_C values, including the merging of some diffraction peaks, disappearance of some weak peaks, and relative intensity changes of some peaks, from LT to HT, corresponding to the elevation in structure symmetry. The experimental patterns matched the simulated ones based on the single crystal structures of different phases, confirming the phase transitions, and the T_C values determined by VT PXRD are within 350–360 K (**1Mn** and **2Zn**), 380–390 K (**3Co**), and 340–350 K (**4Mg**) (Table 2). The VT PXRD patterns could also provide the thermal stability for the powders of the materials, up to the T_d values, *ca.* 410 K (**1Mn**), 360 K (**2Zn**), 410 K (**3Co**), and 440 K (**4Mg**). These data agree with the thermal analyses. It is worth mentioning that the powder samples of **2Zn** to **3Co** decomposed shortly after their phase transition, but the single crystals showed better thermal stability. For example, we have successfully collected intensity data for a single crystal of **2Zn** at 375 K, 15 K higher than the T_d = 360 K observed for powder.

Crystal structures and the relevant negative thermal expansion

The crystal structures of the ordered LT phase and the disordered HT phase were determined (Table 1, Table S1†) by SXRD. **1Mn** and **2Zn** are perovskites (Fig. 2), as are those of [AmineH][M(HCOO)$_3$] for mono-ammonium ions with 2–4 non-H atoms,[24–27,29,31,32] while **3Co** and **4Mg** possess the chiral metal–formate networks (Fig. 3) as do those of $[NH_4][M(HCOO)_3]$,[23] $K[M(HCOO)_3]$[46] and the very recently reported $[HONH_3][M(HCOO)_3]$ series.[33] They all displayed significant ATE/NTE accompanying the phase transition.

The isostructural perovskites **1Mn** and **2Zn** possess the anionic NaCl-frameworks of $[M(HCOO)_3^-]$ with the cubic cavities occupied by the $NH_2NH_3^+$ cations (Fig. 2). Their LT phases belong to the polar orthorhombic space group $Pna2_1$. In the structures, each octahedral metal ion connects to six neighboring metal ions in an octahedral spatial arrangement, through six *anti–anti* formates, thus forming a metal–formate framework with a topology of $4^{12}\cdot6^3$ (Fig. 2a and 2b). At RT (Table S2†), the M–O distances are 2.178(2)–2.196(2) Å for **1Mn**, and 2.099(2)–2.115(2) Å for **2Zn**, respectively, and the *cis*- O–M–O angles are 86.37(7)–94.43(9)°, and the *trans*- O–M–O angles are 176.10(8)–179.08(8)°. The framework grid or cavity has M–OCHO–M edges of 5.908–5.951 and 5.791–5.817 Å for **1Mn** and **2Zn**, respectively. These data are comparable with other known perovskite AMFFs,[24–27,29,31] and the decrease in the lattice dimensions and interatomic distances of M–O and M···M from **1Mn** to **2Zn** is in good agreement with the metal ionic radii.[47] The grid is somewhat

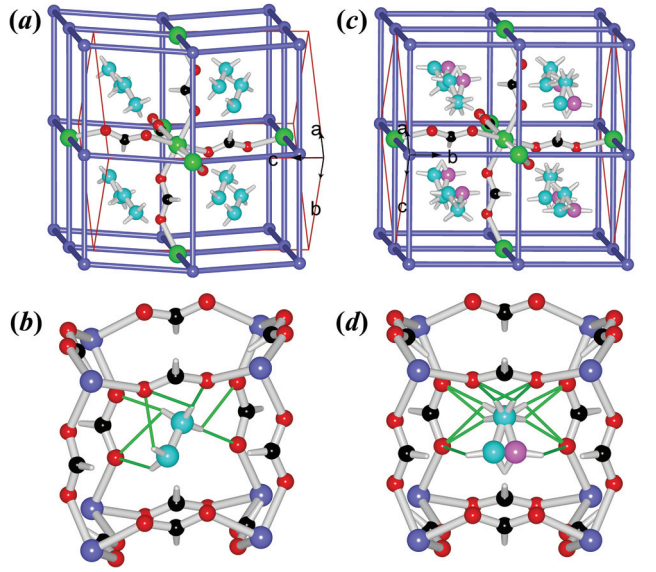

Fig. 2 The structure of **1Mn**: (a) and (b) at 290 K, (c) and (d) at 400 K. The frameworks (a and c) are in topological views, with one Mn connecting to its six neighbors by *anti–anti* formates, showing a octahedral spatial arrangement (large green Mn), and the details about the cavities and the $NH_2NH_3^+$ cations are shown in (b) and (d), with the thin green bonds representing the N–H···O HBs. Color scheme: Mn violet-blue/green, C black, H white, O red, N cyan/pink, and violet-blue sticks for $HCOO^-$ in (a) and (c).

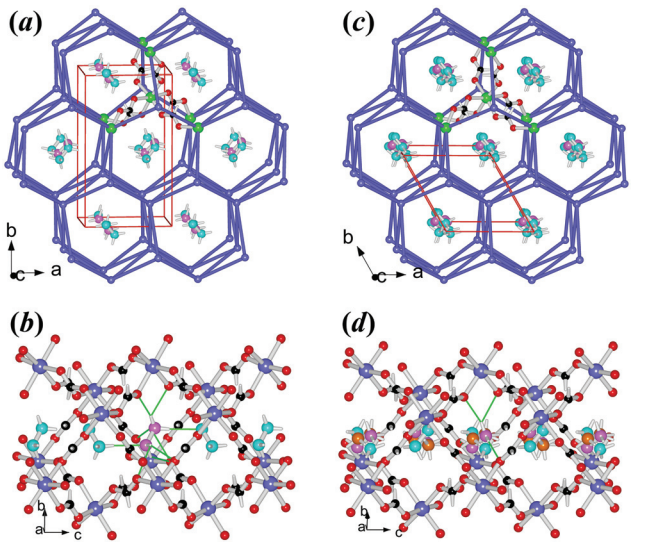

Fig. 3 The structure of **3Co**: (a) and (b) at 290 K, (c) and (d) at 405 K. The frameworks (a and c) are in topological views, with one Co connecting to its six neighbors by *anti–anti* formats, forming a centered trigonal prism (large green Co), and the details about the framework channels and the $NH_2NH_3^+$ cations are shown in (b) and (d), with the thin green bonds representing the N–H···O HBs. Color scheme: Co violet-blue/green, C black, H white, O red, N cyan/pink/orange, and violet-blue sticks for $HCOO^-$ in (a) and (c).

slanted, with the M–OCHO–M grid edges running along the *c* axis and the two diagonal directions of the *ab* plane. The cavity volumes are 44.4 (**1Mn**) and 40.1 (**2Zn**) Å^3, calculated by PLATON (Fig. S7†).[48] These allow accommodation of the $NH_2NH_3^+$ cation with its vdW volume of 44 Å^3 estimated by PCModel 9.1.[49] In the cavity, the $NH_2NH_3^+$ cation has its long axis nearly lying on the longest body-diagonal of the cavity, and forms several N–H···O HBs to the anionic framework. Each N–H donor of the NH_3^+ site of the cation forms one short (strong) and one long (weak) N–H···O HBs with the two O atoms from one formate, and the HB geometries are: for **1Mn**, N···O distances 2.876(3)–2.926(4)/2.990(4)–3.110(3) Å, N–H···O angles 164.9–173.4/114.5–121.7°; for **2Zn**, 2.878(4)–2.944(4)/2.970(4)–3.088(4) Å and 165.3–171.0/117.4–122.5°. Instead, each N–H donor of the NH_2 site forms only one long, weak N–H···O_{HCOO} HB with N···O distances 3.034(4)–3.125(4) Å and N–H···O_{HCOO} angles 133.0–139.8°. Therefore, the neutral NH_2 site is loosely bonded comparing to the positive NH_3^+ site. The NH_2 end is also inclined to one side of the cavity, leaving the other side empty but available for forming alternative HBs. This asymmetry is very different from the mirror symmetric HBs and cation–cavity relationship in the very closely related $[CH_3NH_3][M(HCOO)_3]$ perovskites[24] showing no phase transitions above 180 K. The loosely bonded NH_2 end and its asymmetric environment provide the possibility of movement at this end upon warming, as observed in the HT phases. In the framework the metal arrays along the *c* direction are slightly wavy, and all $NH_2NH_3^+$ cations have their NH_3^+ sites aslant towards the $-c$ direction. These are compatible with the polar space group $Pna2_1$ and the lack of mirror in the *c* direction. On cooling down to 110 K the LT structures remain unchanged, with small decreases in cell dimensions and bond distances (Fig. S8a,† Table S2†). Therefore the LT structures are polar, and the polarization should be along the *c* axis. Indeed, if the planes of the metal atoms, perpendicular to the *c* axis, are considered as the average, symmetric planes for the distribution of the negative charges of the framework, all $NH_2NH_3^+$ cations have their positive NH_3^+ ends showing unequal out-of-plane distances from the two such planes on both sides of the NH_3^+ end, resulting in shifts, 0.457 Å for **1Mn** and 0.417 Å for **2Zn**, calculated from the 110 K structures, towards the $-c$ direction with respect to the anionic framework. Assuming that the NH_3^+ ends are the positive point charges located at the N atoms,[23a,b,50] these shifts generate dipoles, 4 per unit cell and parallel to each other, and the spontaneous polarization could be estimated at 3.58 (**1Mn**) and 3.48 (**2Zn**) μC cm^{-2} at 110 K (Table 2), which is typical for molecular ferroelectrics,[11,20] along the $-c$ direction.

The structures of the HT phases of **1Mn** at 400 K and **2Zn** at 375 K, all above the phase transition temperatures (Table 2), are centrosymmetric, in the space group *Pnma*, by addition of the mirror along the *b* direction of the HT lattices, *i.e.* the *c* direction of the LT lattices, as the relationship between the LT and HT conventional cells for both crystals is $a^{HT} \approx a^{LT}$, $b^{HT} \approx c^{LT}$ and $c^{HT} \approx -b^{LT}$. In the HT structures (Fig. 2c and 2d), while the metal–formate frameworks remain unchanged in their topology, the differences in interatomic distances of M–O and M···M become smaller (Table S2†), and the wavy metal arrays in the LT structures are now straight. The most remarkable change in the structures is that the $NH_2NH_3^+$ cation shows two orientations in the HT phases, with its NH_2 end splitting into two positions on the two sides of the mirror along the *b* direction. In fact this disorder, or the librational movement of the NH_2 end, introduces the mirror symmetry and thus the centrosymmetry for the HT phase. The $NH_2NH_3^+$ cation now behaves as a pendulum, a property reminiscent of pendulum-type molecular ferroelectrics.[35] Its NH_3^+ site is anchored by six N–H···O_{HCOO} HBs (N···O 2.928(3)–3.107(3) Å, N–H···O_{HCOO} 117–169°), but the NH_2 end can vibrate. However, the $NH_2NH_3^+$ pendulum does not simply vibrate forward and back. At HT, the vibration locus of the NH_2 end across the mirror plane is, in fact, an arc (or a flat V-shape), as shown by the two mirror-symmetric elongated thermal ellipsoids, with the locus plane approximately perpendicular to the N–N bond (Fig. S9a†). The temperature evolution of the N ellipsoids from LT to HT also revealed that the gradually enhanced thermally agitated movements, perpendicular to the N–N bond for the NH_2 end, but approximately along the N–N bond for the NH_3^+, finally led to the librational motion and the caused HB alternations. The two NH_2 sites are separated 0.74–0.75 Å, so the vibration amplitude of the NH_2 end is 0.37 Å, which corresponds to the distance between NH_2 and the mirror plane. The two materials showed ATE behavior during the transition (Fig. S8a,† Table 3). The *b* and *c* axes (in LT cell setting) expand *ca.* 0.1 Å or 1% from 290 K to *ca.* 400 K, but the *a* axis contracts *ca.* 0.1 Å or 1%, resulting in NTE along the *a* direction. In fact the contraction of *a* axis might start from a lower temperature of 200 K. The coefficients of the thermal expansion (CTE, or α), negative or positive, are around 100×10^{-6} K^{-1}, estimated by currently available data, and these are classified as "colossal".[15b] This behavior could be explained by the librational movement of $NH_2NH_3^+$ in the *c* direction with its long molecular axis lying approximately along the *a* direction, and the conformation adaptability of the metal–formate frameworks. The N–N distances are shortened *ca.* 0.03 Å from LT to HT, reflecting such librational motion. NTE has been observed in many classes of framework materials,[13–16] such as oxides and zeolites[14] (*e.g.*, ZrW_2O_8 and AlPOs), cyanides[15] (*e.g.*, $Zn(CN)_2$ and $Ag_3[Co(CN)_6]$), and MOFs[16] (*e.g.*, MOF-5 and HKUST-1), and the mechanism is thought to consist mainly of the transverse rigid unit modes or the transverse vibration of the linkages.[13] The cavity volumes increase quite significantly, 52.8 (**1Mn**) and 45.2 (**2Zn**) Å^3, compared to 44.4 (**1Mn**) and 40.1 (**2Zn**) Å^3 of the LT phases at RT (Fig. S7†). The framework cavity becomes more regular (Fig. 2d *vs.* 2b). From these observations, we suggest that upon heating the expansion of the framework and the change in cavity shape and size and HBs allows first the vibration of the loosely HB-bonded NH_2 end of the $NH_2NH_3^+$ pendulum, then the contraction of the framework along the *a* direction but still an expansion along *b* and *c*, to fit such librational motion. This indicates a double potential well with a small energy barrier for the $NH_2NH_3^+$

Table 3 The anisotropic coefficient of thermal expansion (α_l, in 10^{-6} K^{-1}) for the four materials[a]

Compound	**1Mn**			**2Zn**		
T range (K)	110–200	200–290	290–400	110–200	200–290	290–375
α_a	23	−7	−96	21	−7	−108
α_b	3	27	97	11	36	148
α_c	25	45	86	22	41	98
α_V	51	65	86	55	69	138
Compound	**3Co**			**4Mg**		
T range (K)	110–200	200–290	290–405	110–200	200–290	290–400
α_a	−3	−10	−20	−10	−6	−11
α_{bO}	10	19	−100	15	9	−89
α_{bH}	7	12	−81	9	5	−69
α_c	13	39	173	27	43	171
α_V	20	48	56	32	46	72

[a] The values were calculated through the equation $\alpha_l = \Delta l/(\Delta T \times l_{av})$ using the data at the two neighbor temperatures. For **1Mn** and **2Zn**, the cell settings of the HT phases were chosen as the same as the LT phases. For **3Co** and **4Mg**, a and c axes are the same for LT and HT phases, but for the b axis two settings, orthorhombic (bO) for LT and hexagonal (bH) for HT, were included. The accuracies were estimated at a few 10^{-6} K^{-1} in most cases.

pendulum at HT. While in LT, this vibration is frozen. The fact that the LT phases have a polar space group $Pna2_1$ but the HT phases belong to the non-polar, centro-symmetric space group *Pnma* is of interest for ferroelectricity because such change, from *Pnma* to $Pna2_1$, implies the ferroelectric phase transitions on cooling, for **1Mn** and **2Zn**, with the Aizu notation *mmmFmm*2.[51] The higher N values of 3.7 (**1Mn**) and 3.2 (**2Zn**) by DSC studies indicate that the framework changes, from somewhat wavy one at LT to more regular straight one at HT, together with small twists in the orientation of formate bridges, should have the extra contribution to the N values. This is because the order–disorder transition of the cation, two discrete states in HT structures but one in LT, solely gives the ratio of states, $N = 2$.

3Co and **4Mg** are isostructural (Table 1, S1c, S1d†), possessing a chiral metal–formate framework of $4^9{\cdot}6^6$ topology (Fig. 3), with hexagonal channels occupied by the $NH_2NH_3^+$ cations. As mentioned above, the occurrence of two different metal–formate frameworks within the present series is quite unusual. One possible reason is the size of $NH_2NH_3^+$, with its vdW volume of 44 Å^3, between the relevant ammonium ions,[49] 25 Å^3 of NH_4^+ and 38 Å^3 of $HONH_3^+$ for $4^9{\cdot}6^6$ frameworks, and 53 Å^3 of $CH_3NH_3^+$ or above of other larger mono-ammonium ions for $4^{12}{\cdot}6^3$ ones. The LT structures of **3Co** and **4Mg** belong to chiral orthorhombic space group $P2_12_12_1$, same as our recently published $[HONH_3][M(HCOO)_3]$ series,[33] and possess quite similar lattice dimensions too (noting that in the present case the c axes are equivalent to the b axes in the $[HONH_3][M(HCOO)_3]$ series). However, no phase transitions have been detected for the $[HONH_3][M(HCOO)_3]$ series. Similarly, in **3Co** and **4Mg**, each octahedral metal node is connected to six neighbors *via* the *anti–anti* formate linkages, making up the centered trigonal prism within the frameworks (Fig. 3a). The MO_6 octahedron has M–O distances of 2.054(1)–2.122(2) Å, *cis*-O–M–O angles of 80.62(7)–96.01(7)°, and *trans*- O–M–O angles of 171.35(7)–176.14(5)° (Table S3,† at RT), similar to the reported data for other relevant Co or Mg AMFF compounds.[23,33] The frameworks possess slightly compressed hexagonal channels running along the c direction. In the channel (Fig. 3b) the $NH_2NH_3^+$ cations are arranged side by side but aslant with respect to the c direction, showing a tilting angle of 65° between the molecular axes and the c direction, and the adjacent cations are oriented up and down. This is significantly different from the $[HONH_3][M(HCOO)_3]$ series, in which the head to tail arranged $HONH_3^+$ cations in the channel have tilting angles of 21°. The shorter c axes of **3Co** and **4Mg** than the equivalent b axes of the $[HONH_3]$-$[M(HCOO)_3]$ series are compatible with this difference. Two N–H donors of the NH_3^+ end form four N–H···O HBs to the metal–formate framework with N···O = 2.824(2)–2.945(2) Å, N–H···O angles 118.6–165.8°; and the left N–H donor points to the long electron pair of the NH_2 end of the adjacent cation, with N···N = 3.058–3.084 Å, and N–H···N angles of 172.9–176.4°. Whether this N–H···N interaction is a HB or a pseudo HB[33,52] merits further investigation. The NH_2 end forms N–H···O HBs to the framework, with N···O = 2.946(2)–3.379(2) Å, and N–H···O angles of 101–146°, indicating weaker HB strengths compared to the NH_3^+ site. The strengths of cation–framework HBs involved in **3Co** and **4Mg** are weaker than those observed in the $[HONH_3][M(HCOO)_3]$ series, in which a strong O–H···O HB between $HONH_3^+$ and the framework probably prohibits the structural phase transition. In the framework the formato-bridged M···M distances are 5.820–5.988 Å (Table S3†), larger than those of the perovskites (Table S2†) and the void spaces that the frameworks provide for each $NH_2NH_3^+$ are 49.7 (**3Co**) and 53.2 (**4Mg**) Å^3. Surprisingly, these void spaces are larger than those found in **1Mn** and **2Zn** (Fig. S7†), and the framework is expanded. In fact, in the present series, the perovskite frameworks are denser than the chiral frameworks when considering the cell volumes, all per 4 formula of $[NH_2NH_3]$-$[M(HCOO)_3]$, and packing coefficients,[53] 807.3 (**3Co**) and 807.6 (**4Mg**) *vs.* 776.2 (**2Zn**) Å^3 and 0.710 (**3Co**) and 0.705 (**4Mg**) *vs.* 0.745 (**2Zn**), considering that the three divalent metal ions have very close radii.[47] This is quite unexpected because in our

previous work we have observed that the chiral $4^9{\cdot}6^6$ frameworks should be denser than perovskite frameworks.[21,33] The framework expansion of the chiral $4^9{\cdot}6^6$ frameworks *vs.* the perovskites within the series is due to the significant enlargement of the M–O–C angles of **3Co** and **4Mg**, 121.4(2)–131.9(1)°, compared with **1Mn** and **2Zn**, 118.2(2)–123.4(2)°, the change in these angles indicating again the breathing nature of the framework.[24,54] The LT structures remained unchanged down to 110 K, showing a small decrease in *b*, *c*, *V* of the cell dimensions but a slight increase in *a*, thus NTE in the *a* direction (Table 3, Fig. S8b†), and a very slight decrease in the interatomic distances (Table S3†). The LT structures in $P2_12_12_1$ belong to the non-polar D_2 point group. However, the polarization properties merit to be discussed here. In fact, in one channel shown in Fig. 3b of the LT phase, the cations are tilting up and down, and their NH_3^+ ends shift slightly to $+c$ and the NH_2 ends to $-c$ with respect to the framework. This could result in a net, small dipole in the channel along the *c* direction, and the channels arranged along the *a* axis include the cations in the same tilting arrangement. Thus, these channels together with the cations forming a layer have the same polarization direction. However, the channels packing along the *b* direction contain $NH_2NH_3^+$ cations in different tilting directions, related by the 2_1 axis, thus resulting in anti-parallel arranged dipoles. Therefore, **3Co** and **4Mg** are antiferroelectrics[20] in LT.

After their phase transitions (Table 2), the two materials are still isostructural (Table 1, S1c, S1d,† Fig. 3c and 3d). The structures at 405 K for **3Co** and 400 K for **4Mg** revealed that the two materials underwent several remarkable changes from LT to HT in their symmetry, lattice, and orientations of the $NH_2NH_3^+$ cations in the framework channel, though the framework topology remained unchanged. The space group changed from non-polar orthorhombic $P2_12_12_1$ (LT) to polar hexagonal $P6_3$ (HT), and the HT unit cells doubly reduced compared to the LT ones, with a relationship of $a^{HT} \approx a^{LT}$, $b^{HT} \approx (b^{LT} - a^{LT})/2$ and $c^{HT} \approx c^{LT}$, then $V^{HT} \approx V^{LT}/2$. In fact, if the primitive LT cell is added a *C*-center, the resultant *C*-centered lattice has a primitive cell with the following dimensions: for **3Co**, a = 7.9341, b_H = 7.9893, c = 7.3361 Å, $\alpha = \beta = 90°$, $\gamma = 119.77°$, and V = 403.7 Å^3 and for **4Mg**, a = 7.8888, b_H = 7.9391, c = 7.4295 Å, $\alpha = \beta = 90°$, $\gamma = 119.79°$; and V = 403.8 Å^3. These data are metrically very close to the hexagonal HT cells. Therefore, the HT cell is derived by the addition of *C*-centers upon the primitive orthorhombic LT cell, together with *a*/*b* shrinking but *c* expanding (Fig. S8b,† Table 3). The α values are close to -100×10^{-6} K^{-1} in the *b* direction, and 170×10^{-6} K^{-1} for the *c* directions. These data are all quite large.[11] The frameworks become regularly hexagonal, and expand slightly, with fewer unique molecular geometries, by minor framework modulation. The void spaces for each $NH_2NH_3^+$ are 51.0 (**3Co**) and 54.5 (**4Mg**) Å^3, only 1.3 Å^3 larger than those in LT phases, quite different from the perovskites **1Mn** and **2Zn** showing more enlargements (Fig. S7†). The $NH_2NH_3^+$ cation becomes trigonally disordered, with triplet orientations related by the 6_3 axis, and the molecular axis of $NH_2NH_3^+$ is more inclined to the *c* direction with a tilting angle of 52°, compatible with the ATE in cell dimensions (*a*/*b* shrinking and *c* expanding) from LT to HT. After the phase transition the motion of the cation increased more significantly, as indicated by the more enlarged thermal ellipsoids, and the thermal ellipsoids of the O atoms of formate became more disk-like, indicating the coupling of the framework with the disordered state of $NH_2NH_3^+$ (Fig. S9b†). Again, it seems that the order–disorder transition of $NH_2NH_3^+$ and the conformity or flexibility of the metal–formate frameworks to fit such transition contribute to the ATE. Such anisotropic changes in cell dimensions are a reversal of the behaviour observed for the $[NH_4][M(HCOO)_3]$[23a,b] series, where *a*/*b* expanded and *c* shrank, with the same framework topology but different librational motion or disordered state of the cation. In fact, in $[NH_4][M(HCOO)_3]$ the NH_4^+ cation oscillates along the *c* direction. Fewer and weaker HBs are observed for each orientation of $NH_2NH_3^+$ as we countered 3 rational N–H···O HBs for the NH_3^+ end with longer N···O distances and probably only one for the NH_2 end, and the N–H···N contacts between two adjacent cations are not favorable because the N–H groups are more or less oriented towards one another. Now in the polar HT structures the NH_3^+ ends of all cations shift toward $+c$, and the shifts are 0.331 and 0.437 Å for **3Co** and **4Mg** respectively, as calculated by the HT structures. In the same way as we did for $[NH_4][M(HCOO)_3]$,[23a,b] by these shifts we calculated polarization values of 2.61 and 3.44 μC cm^{-2} for **3Co** and **4Mg** respectively in their HT phases (Table 2). Therefore, from the above structural information, the phase transitions for the two materials from LT to HT are probably antiferro- to ferroelectric. Since the framework has minor changes during the transition, the *N* values of 2.7 (**3Co**) and 2.5 (**4Mg**) could be considered solely as the results of three discrete states of the trigonally disordered cation in the HT structures *vs.* one state of ordered cation in the LT phases, with a ratio of $N = 3$.

The structure investigation revealed that phase transitions occurring in the present materials are all order–disorder like, triggered by the thermally activated motions of the $NH_2NH_3^+$ cation and the accompanied framework modulations. Upon heating, for the perovskites of **1Mn** and **2Zn** the framework expansion and change are significant, but for the chiral **3Co** and **4Mg** the framework alterations are small. The significant ATE including NTE for these materials is due to the librational motion of $NH_2NH_3^+$ and the conformity and adaptability of the metal–formate frameworks to match such motion. This coupling between the cations and anionic frameworks probably provides a new mechanism for NTE of MOFs, because the guests or cations usually dampen NTE,[17] but this does not seem to be the case for the present AMFFs. We also think that the middle size of $NH_2NH_3^+$ and its characteristics in forming HBs have resulted in such interesting series with two typical AMFF structures.

Dielectric properties and their relevance to structure transitions

The temperature-dependent dielectric permittivity (dielectric constant ε' and loss tanδ) of the four materials were

investigated. The T_d values of **1Mn** and **4Mg** are *ca.* 50 K and 90 K higher than their T_C values, whereas T_d values for **2Zn** and **3Co** are *ca.* 20 K higher than their T_C values (Table 2). Therefore, the dielectric responses and anomalies of the **1Mn** and **4Mg** corresponding to the phase transitions could be studied with fair reliability, and we focused on these two materials. For **2Zn** and **3Co** the thermal decomposition is quite close to the phase transition, so their dielectric properties are briefly discussed.

The ε'/tanδ *vs.* T traces of **1Mn** at 1, 10, 100 and 1000 kHz are shown in Fig. 4a. On heating, the ε' value at 1 MHz increased slowly from 7.0 around 280 K to 10.4 at the turning point of 353 K (Table 2), which is close to the T_C, then it rose to the quite sharp maximum of 28.0 around 364 K, and went down on further heating, first quickly then slowly, to 14.3 around 390 K. After that the trace showed a small peak around 395 K, then started to rise, and above 410 K it went up more rapidly due to thermal decomposition of the sample. The tanδ data (Fig. 4a, inset) showed the related step around 365 K and the rise around 390 K then the enhancement above 400 K. When the frequency (f) was lowered, the ε' peak values

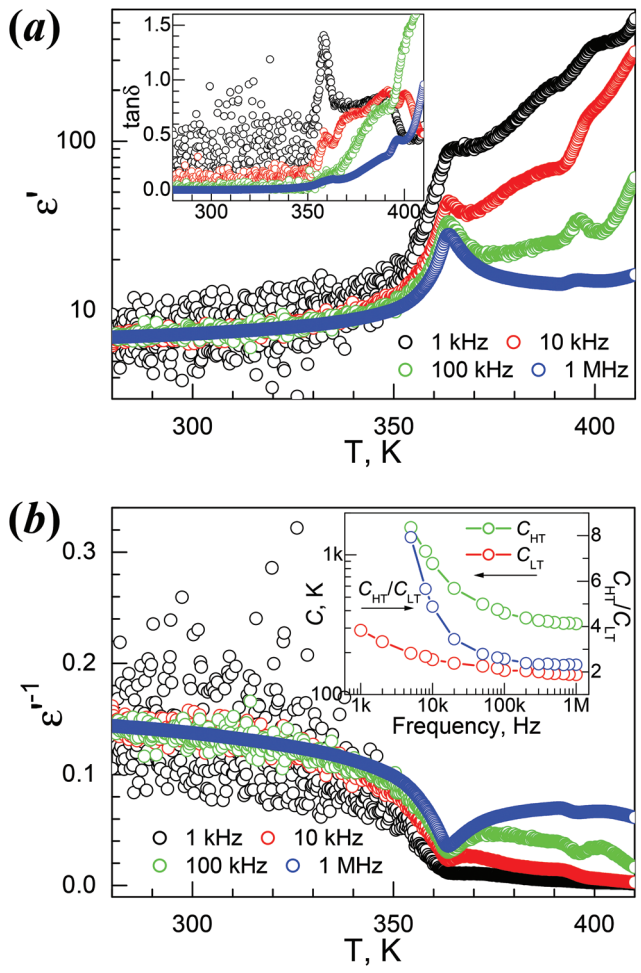

Fig. 4 Temperature-dependent traces of the dielectric permittivities on heating for **1Mn**: (a) ε' *vs.* T, and (inset) tanδ *vs.* T, (b) the relevant $1/\varepsilon'$ *vs.* T plots, and (inset) the plots of C_{LT}, C_{HT} and C_{HT}/C_{LT} ratio *vs.* frequency.

around 364 K increased to 33, 42, 71 and 260 for 100, 10, 1 and 0.1 kHz. The reciprocal permittivity $1/\varepsilon'$ *vs.* T plots (Fig. 4b) showed a V-shape around 364 K, allowing the application of the Curie–Weiss laws $\varepsilon' = C/(T - T_0)$ for the HT side and $\varepsilon' = C/(T_0 - T)$ for the LT side, affording the C/T_0 data in K at 1 MHz, $3.2 \times 10^2/353$ and $1.4 \times 10^2/368$, and the C_{HT}/C_{LT} ratio 2.3. The C values are typical for molecular ferroelectrics undergoing disorder–order transitions of HB systems,[11,12,20] and the T_0 data are close to the T_C. These data remained nearly unchanged for f values above 100 kHz (Fig. 4b, inset), and the C_{HT}/C_{LT} ratios of 2.3 to 2.6 indicated the possible second order ferro- to para-electric phase transition according to the Devonshire theory.[20b] Below 100 kHz, the C values and C_{HT}/C_{LT} ratios increased, but the T_0 data changed a little. The prominent dielectric anomaly around 364 K is clearly related to the phase transition at 355 K, triggered by the order–disorder transition of the $NH_2NH_3^+$ cation, as discussed before. In the HT para-electric state, the $NH_2NH_3^+$ cation has its NH_2 end quickly vibrating between two mirror-related positions. When the temperature is lowered, this librational movement is frozen and the material undergoes a para- to ferro-electric phase transition, leading to the polar LT phase.

4Mg displayed strong frequency dispersion and quite complicated behavior in its dielectric responses and anomalies (Fig. 5, Fig. S10,† Table 2). At 1 MHz, the ε' *vs.* T trace, starting from 7.9 at 280 K, gradually increased to show a first rise step in 335–355 K (ε' = 10–14), then a second rise step from 355 to 375 K (ε' = 14–24), then continuously went up to a maximum of 40.3 around 430 K. After a shallow minimum of 38.6 around 435 K, the trace rose again, probably caused by thermal decomposition (Fig. 5a). The derivative dε'/dT plot (Fig. 5a, inset) displayed three maxima at 340, 364 and 415 K, indicating the three increase steps in ε'. The tanδ *vs.* T trace at 1 MHz (Fig. 5b) possesses very similar stepwise characteristics. These data revealed complicated two or three steps phase transitions, as observed in the DSC study. For lower f values, the rise in ε' shifted to lower temperatures, the ε' values increased greatly, and the rise step around 370 K in fact became a broad peak with an ε' value of up to 2.3×10^3 for 100 Hz. Below 1 kHz, the ε' values are high above 370 K. The $1/\varepsilon'$ *vs.* T plots (Fig. S10a†) are stepwise, and basically include two straight segments in 390–420 K (I) and 350–370 K (II). The data at 1 MHz within these two segments fitted by the Curie–Weiss law $\varepsilon' = C/(T_0 - T)$ resulted in the C/T_0 in K, $3.4 \times 10^3/508$ and $5.4 \times 10^2/393$ for segments I and II, respectively (Table 2). These C values are rational,[11,12,20] and the T_0 values are higher than T_C. Strong frequency dependence is clearly observed for the tanδ data shown in Fig. 5b and Fig. S10b.† At 100 Hz, a peak in the tanδ *vs.* T plot was observed at 346 K. With increasing f values, the peak temperatures shifted higher, and became asymmetric by the emergence of two shoulders, a small one on the left and a large one on the right. The right shoulder developed to broad peaks approaching 430 K for f values higher than 2 kHz, and at the same time the original high peaks observed for lower f values were gradually suppressed into low shoulders. All these results revealed the relaxor-like behavior of **4Mg**,[23b,26a,55,56]

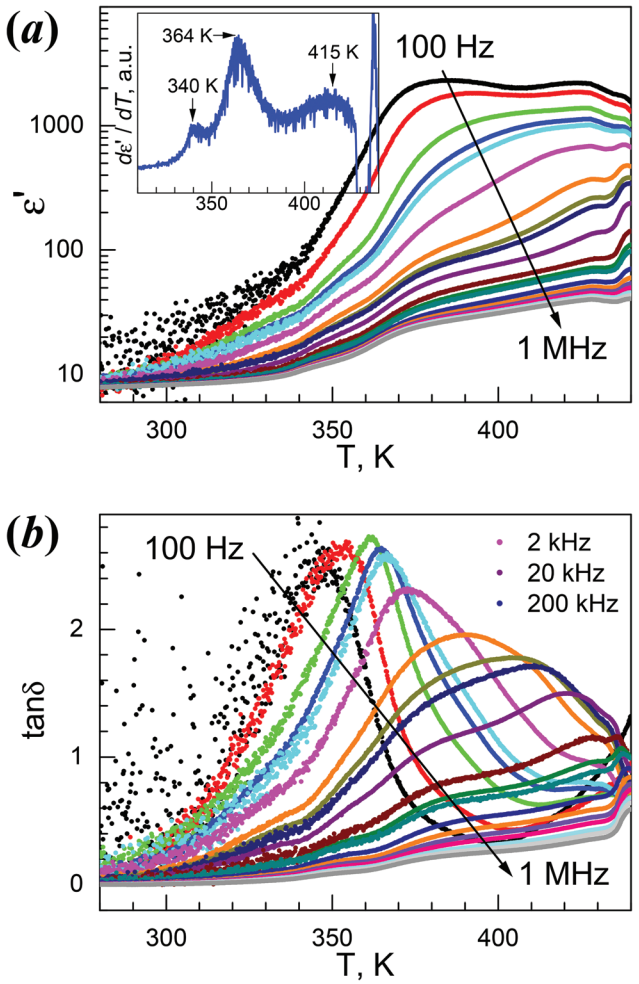

Fig. 5 Temperature-dependent traces of the dielectric permittivities on heating for **4Mg**: (a) ε' *vs. T*, and inset dε'/d*T* plot at 1 MHz, (b) tanδ *vs. T*.

and there are seemingly two dielectric relaxation processes, one around 360 K at low *f* values and the other around 420 K at high *f* values. In the isothermal tanδ *vs. f* traces from 336 K to 436 K in 4 K spaces (Fig. S10b†), the frequency dependence is significant, but the two relaxation processes are not easy to distinguish. However, the log–log plots showed the power law tan$\delta \sim f^n$ for low and high frequency sides of the peak positions, and typically, for the data of a temperature of 380 K, the exponents were n = 0.65 and −0.41 for both sides. These represent Jonscher's universal relaxation law for dielectrics,[57] relating to the local transition in the orientation of the $NH_2NH_3^+$ cation and the spread or relaxation in the lattice of the initial transition. The dielectric relaxation observed around 360 K at low *f* values obeyed the Arrhenius law for the $\tau = (2\pi f)^{-1}$ *vs.* T_P (temperature at peak position) data below 2 kHz where T_P is located in the ε'' *vs. T* data, with a pre-exponential factor $\tau_0 = 1.45 \times 10^{-17}$ s and an activation energy $E_a/k_B = 1.19 \times 10^4$ K ∼ 1.03 eV (Fig. S10b,† inset). However, the relaxation processes around 420 K and at high *f* values could not be parameterized because of the broad shoulder or peaks and the temperature very close to T_d.

The dielectric response of **4Mg** could be understood based on the VT structures discussed before. In the LT phase, the cations are completely ordered in the lattice and the LT phase is antiferroelectric, thus the material displayed low dielectric response. On heating, the weak strengths of cation-framework HBs and somewhat large void framework space allow the cation to become trigonally disordered. The HT structure is polar, with all NH_3^+ ends of the cations shifting to the +*c* direction. The polar character and the disorder of the $NH_2NH_3^+$ cation in the HT structure satisfied the requirements for relaxor ferroelectrics,[56] therefore resulting in the observed dielectric responses of high ε' values in low *f* values and strong frequency dispersion. The activation energy for the cation's movement between different orientations is E_a ∼ 1.03 eV, as revealed by Arrhenius fitting for the frequency dependence around 360 K. This fairly high activation energy might be related to the antiferro- to ferroelectric phase transition and the observed two or three steps involved. VT structures with fine temperature intervals will be of help to reveal the details. **4Mg** might experience another phase transition above 420 K because of the observation of the peaks in both ε'' *vs. T* and tanδ *vs. T* traces, and this might be ferro- to para-electric, though no further information could be obtained due to sample decomposition.

2Zn and **3Co** showed the relevant dielectric anomaly shoulders around their T_C values, as shown in Fig. S11† (**2Zn**) and Fig. S12† (**3Co**). Since their T_C values are close to the T_d values, the dielectric anomalies were superimposed by the further enhanced dielectric responses due to the decomposition subsequently occurred. However, some information could still be retrieved from the data below T_C, *e.g.* the rational C/T_0 values in K, $3.3 \times 10^2/372$ and $3.3 \times 10^2/405$ at 1 MHz, for **2Zn** and **3Co** respectively. These data are listed in Table 2.

Therefore, the dielectric responses and phase transitions of the four present AMFF materials are clearly related to the order–disorder transition of the $NH_2NH_3^+$ cations within the structures, and their basic relevance has been established. The very prominent dielectric anomalies indicate that the LT phases of **1Mn** and **2Zn**, and the HT phases of **3Co** and **4Mg**, being all polar, are probably ferroelectric, though further experimental investigation such as electric hysteresis measurements will be needed when large crystals are available.

Magnetic properties of 1Mn and 3Co

The temperature evolutions of the direct current (dc) susceptibilities of **1Mn** and **3Co** (plots of χT *vs. T*, Fig. 6a) indicate that the two materials mainly displayed spin-canted AF characters. The χT values at 300 K, 4.39 (**1Mn**) and 3.19 (**3Co**) cm^3 K mol^{-1}, are expected for the two divalent octahedral metal ions.[58] On cooling from 300 K to *ca.* 50 K the χT values decreased slowly. Below 50 K the values of χT decreased quickly to reach the minima, then rose to the maxima and then fell again upon further cooling (Table 4). This suggested the occurrence of spontaneous magnetization or magnetic LRO within the materials. The rise for **3Co** was much steeper, with a high maximum of 45.4 cm^3 K mol^{-1}, similar to

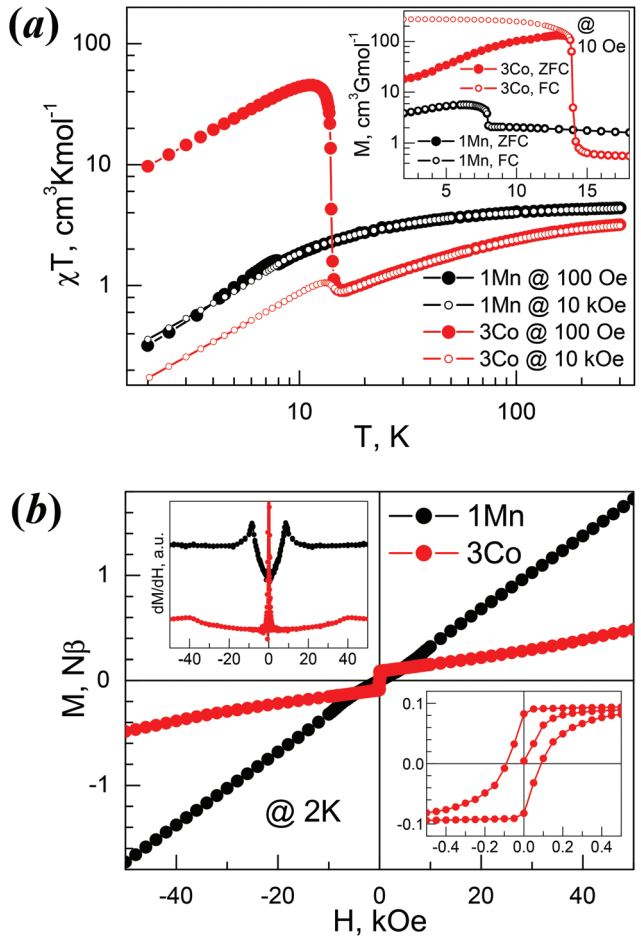

Fig. 6 Magnetism of **1Mn** and **3Co**. (a) Plots of χT *vs.* T under 100 Oe and 10 kOe fields, (inset) the ZFC/FC plots of the **1Mn** and **3Co** under 10 Oe field. (b) Isothermal magnetization plots of **1Mn** and **3Co** at 2 K, (top-left inset) the dM/dH plots, (bottom-right inset) hysteresis loop for **3Co**.

$[HONH_3][Co(HCOO)_3]$.[33] The high temperature susceptibility data obey the Curie–Weiss law well (Fig. S13a†) with Curie constants (C) and Weiss temperatures (Θ) in cm^3 K mol^{-1} and K respectively: 4.57/−13.2 (**1Mn**), 3.80/−56.8 (**3Co**). The Landé g-factors derived from the C values are 2.04 (**1Mn**) and 2.58 (**3Co**), typical for isotropic Mn^{2+} and anisotropic Co^{2+}.[58] These data are comparable to related metal members in other AMFF series,[21] and the significant negative Θ values indicate AF exchange interactions between metal ions, *via anti–anti* formato bridges. Under an applied field of 10 kOe, in high temperature regions the χT traces were almost identical to the traces under a 100 Oe field, while in low temperature regions the rises after the minima were suppressed for **1Mn**, but still observed for **3Co**. These observations characterized the two materials as weak ferromagnets.

The magnetism in the low temperature region for **1Mn** and **3Co** were further investigated by zero-field and field cooled measurements (ZFC/FC, Fig. 6a, inset), isothermal magnetizations (Fig. 6b), and ac susceptibility measurements (Fig. S13b†). The bifurcations in ZFC/FC traces, though not very significant for **1Mn**, indicated the 3D spin-canted AF LRO

Table 4 Summary of magnetic properties of **1Mn** and **3Co**, Curie constants, Weiss constants, listed χT values, and g factors were upon susceptibility data under 100 Oe field, and 10 kOe data in parentheses

Compound	**1Mn**	**3Co**
C[a]/cm^3 K mol^{-1}	4.57 (4.53)	3.80 (3.73)
Θ[b]/K	−13.2 (−12.8)	−56.8 (−55.8)
$(\chi T)_{300\ K}$/cm^3 K mol^{-1}	4.39 (4.36)	3.19 (3.19)
$(\chi T)_{min}$[c]/cm^3 K mol^{-1}, T_{min}/K	1.50, 8.0	0.90, 15.5
$(\chi T)_{max}$[c]/cm^3 K mol^{-1}, T_{max}/K	1.61, 7.8	45.4, 11.5
$(\chi T)_{2\ K}$/cm^3 K mol^{-1}	0.32 (0.36)	9.70 (1.88)
T_N[d]/K	7.9	13.9
T_p[e]/K	8.0	13.8–13.9 13.5–13.8
H_C[f]/kOe (at 2 K)	<0.01	0.09
M_R[g]/$N\beta$ (at 2 K)	<0.001	0.082
$M_{50\ kOe}/N\beta$ (at 2 K)	1.73	0.49
α[h]/°	<0.001	1.10
H_{SP}[i]/kOe (at 2 K)	8.50	>40
J[j]/k_B (K)	−0.38	−3.8
g[k] Factor	2.04 (2.04)	2.85 (2.82)

[a] Curie constants. [b] Weiss constants. [c] Minimum and maximum χT values and the related temperatures. [d] Critical temperatures based on ZFC/FC measurements. [e] Temperatures at peak positions in ac measurements at zero dc field, the first line for in-phase ac response and the second line for out-of-phase response. [f] Coercive fields. [g] Remnant magnetizations. [h] Canting angles, see text. [i] Fields for spin flop from peak or first turn positions in dM/dH. [j] Estimated from $J/k_B = 3\Theta/[2zS(S+1)]$. [k] g Factors derived from Curie constants.

for the two materials at Néel temperatures (T_N) of 7.9 K and 13.9 K for **1Mn** and **3Co**, respectively, determined by the negative peak positions on the dFC/dT data (not given here). For **1Mn**, the spontaneous magnetization was less than 6 cm^3 G mol^{-1}, while **3Co** showed a large spontaneous magnetization of *ca.* 250 cm^3 G mol^{-1}, in agreement with the large χT values at low temperatures. Known AMFFs with large spontaneous magnetizations include **3Co**, chiral $[HONH_3][Co(HCOO)_3]$,[33] perovskite $[C(NH_2)_3][Co(HCOO)_3]$[29a] and niccolite $[CH_3NH_2CH_2CH_2NH_2CH_3][Fe_2(HCOO)_6]$.[34] At 2.0 K (Fig. 6b), **1Mn** showed nearly no hysteresis (remnant magnetization $M_R < 0.001N\beta$ and $H_C < 10$ Oe) but small kinks around 8 kOe (Fig. 6b, top-left inset). In higher fields the magnetization increases linearly and reaches *ca.* $1.7N\beta$ at 50 kOe, being one third of the saturation value of $5N\beta$ for Mn^{2+} ($S = 5/2$ and $g = 2.00$). For **3Co** (Fig. 6b, bottom-right inset), a hysteresis was observed, with M_R and H_C being $0.082N\beta$ and 90 Oe. In the high field region the magnetizations showed a slow increase with a slight turning up around 40 kOe, and the magnetizations were $0.49N\beta$ at 50 kOe. Spin-flop transitions (AF-SP)[59] occurred at 2 K for **1Mn** and **3Co**, and the fields for spin-flop (H_{SP}), estimated by peak position of dM/dH, were 8.5 kOe for **1Mn** and 40 kOe for **3Co**. From the M_R values the canting angle could be estimated at less than 0.001° for **1Mn** and 1.1° for **3Co**, respectively,[59] assuming the existence of two AF interacted sub-lattices in the materials. In ac susceptibilities (Fig. S13b†), **1Mn** displayed frequency-independent peaks in its in-phase (χ') responses at 8.0 K, close to the $T_N = 7.9$ K by dc measurement, while the out-of-phase (χ'') responses were in the noise level. **3Co** showed slight

frequency-dependent χ' and χ'' peaks around 13.8 K, with a small $\phi = (\Delta T_P/T_P)/\Delta(\log f)$[60] ~ 0.004, where T_P is the peak temperature of χ' and f the ac frequency. This relaxation behaviour, similar to that encountered for some Co-AMFFs,[29a,33] could be due to domain-wall movement,[61] or chirality-related ac responses[62] as **3Co** is chiral. The M···M magnetic couplings through the *anti–anti* formato bridge within the two solids could be estimated by using the molecular field result, $J/k_B = 3\Theta/[2zS(S+1)]$, and were −0.38 (**1Mn**) and −3.8 K (**3Co**) for $z = 6$ and $S = 5/2$ and 3/2 for **1Mn** and **3Co**, respectively, and they are comparable to those found in AMFFs.[21] The spin-canted AF is due to the occurrence of Dzyaloshinsky–Moriya or the antisymmetric interaction[63] resulting from the non-centrosymmetric bridges of *anti–anti* HCOO linking magnetic sites, as observed for many AMFFs.[21]

Finally, we emphasize that **1Mn** and **3Co** showed both electric and magnetic LRO in low temperature regions, and this makes the magnetic members of the present series of great interest for the research on MOF/molecule-based multiferroics which were only recognized very recently,[9,23,26,29,30] and probably adds a new family of AMFF multiferroic materials.

Conclusion

In conclusion, we have successfully synthesized and characterized a new class of AMFFs of $[NH_2NH_3][M(HCOO)_3]$ (M = divalent Mn, Zn, Co and Mg) by employing hydrazinium as the cationic template and component. The series has two typical AMFF structures. The Mn and Zn members are perovskites, with anionic $4^{12}\cdot6^3$ metal–formate frameworks and the cubic cavities occupied by the $NH_2NH_3^+$ cations. They undergo structural transitions around 350 K, in which the structures change from LT polar phases in $Pna2_1$ to HT non-polar phases in *Pnma*, due to the occurrence of the librational movement of the NH_2 end of the $NH_2NH_3^+$ cation in the cavity and related significant framework regulation and expansion. The Co and Mg members possess chiral $4^9\cdot6^6$ metal–formate frameworks with chiral hexagonal channels accommodating $NH_2NH_3^+$ cations. The LT phases in non-polar $P2_12_12_1$ are probably antiferroelectric. They display phase transitions at 380 K (Co) and 348 K (Mg) and change to a polar HT phase in $P6_3$ because of the occurrence of trigonal disorder in the cation. Accompanied by these transitions the materials show prominent anisotropic/negative thermal expansion and dielectric anomalies, and their structural relevance is established. From LT to HT, the phase transitions of Mn and Zn members are ferro- to paraelectric, while for the Co and Mg members the transitions are probably antiferro- to ferro-electric. The spontaneous polarization for the polar structures was estimated at 3.58 (Mn, 110 K), 3.48 (Zn, 110 K), 2.61 (Co, 405 K) and 3.44 (Mg, 400 K) μC cm^{-2}. The two magnetic Mn and Co members also show long-range-ordering of spin-canted antiferromagnetism, with Néel temperatures of 7.9 K and 13.9 K, respectively. Therefore, they constitute new molecule-based multiferroics. It is also expected that the present series will produce more than ten new AMFFs showing interesting phase transitions occurring at high temperatures even comparable to the ferroelectric oxides, and the relevant NTE, electric, magnetic and possible multiferroic properties if the two polymorphs for all divalent metal ions from Mn to Zn plus Mg were obtained. The series will probably become a new prototypical class of MOF-based multiferroics, and much further research is required. This research is in progress.

Acknowledgements

This work was supported by the NSFC (grants 21171010, 21290170, 21290171), and the National Basic Research Program of China (grant 2009CB929403).

References

1 (*a*) N. A. Spaldin and M. Fiebig, *Science*, 2005, **309**, 391; (*b*) N. A. Spaldin, S.-W. Cheong and R. Ramesh, *Phys. Today*, 2010, **63**, 38; (*c*) W. Eerenstein, N. D. Mathur and J. F. Scott, *Nature*, 2006, **442**, 759; (*d*) K. F. Wang, J.-M. Liu and Z. F. Ren, *Adv. Phys.*, 2009, **58**, 321; (*e*) M. Mostovoy, *Nat. Mater.*, 2010, **9**, 188.

2 (*a*) S. Dong and J.-M. Liu, *Mod. Phys. Lett. B*, 2012, **26**, 1230004; (*b*) A. Loidl, H. von Loehneysen and G. M. Kalvius, *J. Phys.: Condens. Matter*, 2008, **20**, 430301; (*c*) A. R. Akbashev and A. R. Kaul, *Russ. Chem. Rev.*, 2011, **80**, 1159; (*d*) D. Khomskii, *Physics*, 2009, **2**, 20.

3 (*a*) A. K. Cheetham and C. N. Rao, *Science*, 2007, **318**, 58; (*b*) C. N. Rao, A. K. Cheetham and A. Thirumurugan, *J. Phys.: Condens. Matter*, 2008, **20**, 083202.

4 For recent reviews, (*a*) H.-C. Zhou, J. R. Long and O. M. Yaghi, ed., Thematic issue on metal-organic frameworks, *Chem. Rev.*, 2012, **112**, 673; (*b*) J. R. Long and O. M. Yaghi, ed., Special issue on metal-organic frameworks, *Chem. Soc. Rev.*, 2009, **38**, 1213; (*c*) C. Janiak and J. K. Vieth, *New J. Chem.*, 2010, **34**, 2366.

5 E. Coronado, J. R. Galán-Mascarós, C. J. Gómez-García and V. Laukhin, *Nature*, 2003, **2**, 190.

6 (*a*) O. Sato, J. Tao and Y.-Z. Zhang, *Angew. Chem., Int. Ed.*, 2007, **46**, 2152; (*b*) C. Train, M. Gruselle and M. Verdaguer, *Chem. Soc. Rev.*, 2011, **40**, 3297.

7 P. Dechambenoit and J. R. Long, *Chem. Soc. Rev.*, 2011, **40**, 3249.

8 (*a*) R. Ramesh, *Nature*, 2009, **461**, 1218; (*b*) S.-i. Ohkoshi, H. Tokoro, T. Matsuda, H. Takahashi, H. Irie and K. Hashimoto, *Angew. Chem., Int. Ed.*, 2007, **46**, 3238; (*c*) E. Pardo, C. Train, H. Liu, L.-M. Chamoreau, B. Dkhil, K. Boubekeur, F. Lloret, K. Nakatani, H. Tokoro, S.-i. Ohkoshi and M. Verdaguer, *Angew. Chem., Int. Ed.*, 2012, **51**, 8356; (*d*) H. B. Cui, Z. M. Wang, K. Takahashi, Y. Okano, H. Kobayashi and A. Kobayashi, *J. Am. Chem. Soc.*, 2006, **128**, 15074.

9 I. E. Collings, A. B. Cairns, A. L. Thompson, J. E. Parker, C. C. Tang, M. G. Tucker, J. Catafesta, C. Levelut, J. Haines, V. Dmitriev, P. Pattison and A. L. Goodwin, *J. Am. Chem. Soc.*, 2013, **135**, 7610.

10 (*a*) D.-F. Weng, Z.-M. Wang and S. Gao, *Chem. Soc. Rev.*, 2011, **40**, 3157; (*b*) E. Coronado and K. R. Dunbar, ed., Special issue for the Forum on Molecular Magnetism: The Role of Inorganic Chemistry, *Inorg. Chem.*, 2009, **48**, 3293; (*c*) J. S. Miller and D. Gatteschi, ed., Molecule-based magnets themed issue, *Chem. Soc. Rev.*, 2011, **40**, 3065; (*d*) C. Rovira and J. Veciana, ed., Special issue on crystal engineering in molecular magnetism, *CrystEngComm*, 2009, **11**, 2031.

11 (*a*) T. Hang, W. Zhang, H.-Y. Ye and R.-G. Xiong, *Chem. Soc. Rev.*, 2011, **40**, 3577; (*b*) W. Zhang and R.-G. Xiong, *Chem. Rev.*, 2012, **112**, 1163.

12 (*a*) W. Zhang, Y. Cai, R. G. Xiong, H. Yoshikawa and K. Awaga, *Angew. Chem., Int. Ed.*, 2010, **49**, 6608; (*b*) W. Zhang, H.-Y. Ye, R. Graf, H. W. Spiess, Y.-F. Yao, R.-Q. Zhu and R.-G. Xiong, *J. Am. Chem. Soc.*, 2013, **135**, 5230.

13 (*a*) J. S. O. Evan, *J. Chem. Soc., Dalton Trans.*, 1999, 3317; (*b*) W. Miller, C. W. Smith, D. S. Mackenzie and K. E. Evans, *J. Mater. Sci.*, 2009, **44**, 5441; (*c*) K. Takenaka, *Sci. Technol. Adv. Mater.*, 2012, **13**, 013001; (*d*) C. Lind, *Materials*, 2012, **5**, 1125.

14 (*a*) T. A. Mary, J. S. O. Evans, T. Vogt and A. W. Sleight, *Science*, 1996, **272**, 90; (*b*) G. Ernst, C. Broholm, G. R. Kowach and A. P. Ramirez, *Nature*, 1998, **396**, 147; (*c*) J. S. O. Evans, T. A. Mary, T. Vogt, M. A. Subramanian and A. W. Sleight, *Chem. Mater.*, 1996, **8**, 2809; (*d*) P. Lightfoot, D. A. Woodcock, M. J. Maple, L. A. Villaescusa and P. A. Wright, *J. Mater. Chem.*, 2001, **11**, 212; (*e*) M. P. Attfield and A. W. Sleight, *Chem. Mater.*, 1998, **10**, 2013.

15 (*a*) K. W. Chapman, P. J. Chupas and C. J. Kepert, *J. Am. Chem. Soc.*, 2005, **127**, 15630; (*b*) A. L. Goodwin, M. Calleja, M. J. Conterio, M. T. Dove, J. S. O. Evans, D. A. Keen, L. Peters and M. G. Tucker, *Science*, 2008, **319**, 794.

16 (*a*) N. Lock, Y. Wu, M. Christensen, L. J. Cameron, V. K. Peterson, A. J. Bridgeman, C. J. Kepert and B. B. Iversen, *J. Phys. Chem. C*, 2010, **114**, 16181; (*b*) Y. Wu, A. Kobayashi, G. J. Halder, V. K. Peterson, K. W. Chapman, N. Lock, P. D. Southon and C. J. Kepert, *Angew. Chem., Int. Ed.*, 2008, **47**, 8929; (*c*) V. K. Peterson, G. J. Kearley, Y. Wu, A. J. Ramirez-Cuesta, E. Kemner and C. J. Kepert, *Angew. Chem., Int. Ed.*, 2010, **49**, 585.

17 (*a*) Y.-S. Wei, K.-J. Chen, P.-Q. Liao, B.-Y. Zhu, R.-B. Lin, H.-L. Zhou, B.-Y. Wang, W. Xue, J.-P. Zhang and X.-M. Chen, *Chem. Sci.*, 2013, **4**, 1539; (*b*) I. Grobler, V. J. Smith, P. M. Bhatt, S. A. Herbert and L. J. Barbour, *J. Am. Chem. Soc.*, 2013, **135**, 6411; (*c*) A. L. Goodwin, K. W. Chapman and C. J. Kepert, *J. Am. Chem. Soc.*, 2005, **127**, 17980; (*d*) N. Lock, M. Christensen, C. J. Kepert and B. B. Iversen, *Chem. Commun.*, 2013, **49**, 789; (*e*) A. E. Phillips, A. L. Goodwin, G. J. Halder, P. D. Southon and C. J. Kepert, *Angew. Chem., Int. Ed.*, 2008, **47**, 1396; (*f*) A. E. Phillips, G. J. Halder, K. W. Chapman, A. L. Goodwin and C. J. Kepert, *J. Am. Chem. Soc.*, 2010, **132**, 10.

18 (*a*) R. H. Baughman, S. Stafström, C. Cui and S. O. Dantas, *Science*, 1998, **279**, 1522; (*b*) A. B. Cairns, J. Catafesta, C. Levelut, J. Rouquette, A. van der Lee, L. Peters, A. L. Thompson, V. Dmitriev, J. Haines and A. L. Goodwin, *Nat. Mater.*, 2013, **12**, 212; (*c*) A. B. Cairns, A. Thompson, L. M. G. Tucker, J. Haines and A. L. Goodwin, *J. Am. Chem. Soc.*, 2012, **134**, 445.

19 (*a*) G. N. Greaves, F. Meneau, A. Sapelkin, L. M. Colyer, I. A. Gwynn, S. Wade and G. Sankar, *Nat. Mater.*, 2003, **2**, 622; (*b*) Y. H. Hu and L. Zhang, *Phys. Rev. B: Condens. Matter*, 2010, **81**, 174103; (*c*) K. W. Chapman, G. J. Halder and P. J. Chupas, *J. Am. Chem. Soc.*, 2009, **131**, 17546; (*d*) T. D. Bennett, A. L. Goodwin, M. T. Dove, D. A. Keen, M. G. Tucker, E. R. Barney, A. K. Soper, E. G. Bithell, J.-C. Tan and A. K. Cheetham, *Phys. Rev. Lett.*, 2010, **104**, 115503.

20 (*a*) F. Jona and G. Shirane, *Ferroelectric crystals*, Pergamon Press, New York, 1962; (*b*) M. E. Lines and A. M. Glass, *Principles and Applications of Ferroelectrics and Related Materials*, Clarendon Press, Oxford, 1977; (*c*) T. Mitsui, I. Tatsuzaki and E. Nakamura, *An Introduction to the Physics of Ferroelectrics*, Gordon and Breach Science Publishers, New York, 1976.

21 (*a*) Z. M. Wang, K. L. Hu, S. Gao and H. Kobayashi, *Adv. Mater.*, 2010, **22**, 1526; (*b*) X.-Y. Wang, Z.-M. Wang and S. Gao, *Chem. Commun.*, 2008, 281.

22 (*a*) S. Horiuchi, Y. Tokunaga, G. Giovannetti, S. Picozzi, H. Itoh, R. Shimano, R. Kumai and Y. Tokura, *Nature*, 2010, **463**, 789; (*b*) S. Horiuchi, R. Kumaia and Y. Tokura, *Chem. Commun.*, 2007, 2321.

23 (*a*) G.-C. Xu, X.-M. Ma, L. Zhang, Z.-M. Wang and S. Gao, *J. Am. Chem. Soc.*, 2010, **132**, 9588; (*b*) G.-C. Xu, W. Zhang, X.-M. Ma, Y.-H. Chen, L. Zhang, H.-L. Cai, Z.-M. Wang, R.-G. Xiong and S. Gao, *J. Am. Chem. Soc.*, 2011, **133**, 14948; (*c*) W. Li, M. R. Probert, M. Kosa, T. D. Bennett, A. Thirumurugan, R. P. Burwood, M. Parinello, J. A. K. Howard and A. K. Cheetham, *J. Am. Chem. Soc.*, 2012, **134**, 11940; (*d*) Z. M. Wang, B. Zhang, K. Inoue, H. Fujiwara, T. Otsuka, H. Kobayashi and M. Kurmoo, *Inorg. Chem.*, 2007, **46**, 437.

24 (*a*) Z. M. Wang, B. Zhang, T. Otsuka, K. Inoue, H. Kobayashi and M. Kurmoo, *Dalton Trans.*, 2004, 2209; (*b*) R. Shang, X. Sun, Z.-M. Wang and S. Gao, *Chem.–Asian J.*, 2012, **7**, 1697.

25 X. Y. Wang, L. Gan, S. W. Zhang and S. Gao, *Inorg. Chem.*, 2004, **43**, 4615.

26 (*a*) D.-W. Fu, W. Zhang, H.-L. Cai, Y. Zhang, J.-Z. Ge, R.-G. Xiong, S. D. Huang and T. Nakamura, *Angew. Chem., Int. Ed.*, 2011, **50**, 11947; (*b*) P. Jain, V. Ramachandran, R. J. Clark, H. D. Zhou, B. H. Toby, N. S. Dalal, H. W. Kroto and A. K. Cheetham, *J. Am. Chem. Soc.*, 2009, **131**, 13625; (*c*) M. Sánchez-Andújar, S. Presedo, S. Yáñez-Vilar, S. Castro-García, J. Shamir and M. A. Señarís-Rodríguez,

Inorg. Chem., 2010, **49**, 1510; (*d*) Z. Wang, P. Jain, K.-Y. Choi, J. van Tol, A. K. Cheetham, H. W. Kroto, H.-J. Koo, H. Zhou, J. Hwang, E. S. Choi, M.-H. Whangbo and N. S. Dalal, *Phys. Rev. B: Condens. Matter*, 2013, **87**, 224406; (*e*) R. I. Thomson, P. Jain, A. K. Cheetham and M. A. Carpenter, *Phys. Rev. B: Condens. Matter*, 2012, **86**, 214304; (*f*) W. Wang, L.-Q. Yan, J.-Z. Cong, Y.-L. Zhao, F. Wang, S.-P. Shen, T. Zou, D. Zhang, S.-G. Wang, X.-F. Han and Y. Sun, *Sci. Rep.*, 2013, **3**, 2024, DOI: 10.1038/srep02024.

27 (*a*) B. Zhou, Y. Imai, A. Kobayashi, Z.-M. Wang and H. Kobayashi, *Angew. Chem., Int. Ed.*, 2010, **50**, 11441; (*b*) Y. Imai, B. Zhou, Y. Ito, A. Kobayashi, Z.-M. Wang and H. Kobayashi, *Chem.–Asian J.*, 2012, **7**, 2786.

28 M. Y. Li, B. Liu, B. W. Wang, Z. M. Wang, S. Gao and M. Kurmoo, *Dalton Trans.*, 2011, **40**, 6038.

29 (*a*) K.-L. Hu, M. Kurmoo, Z.-M. Wang and S. Gao, *Chem.–Eur. J.*, 2009, **15**, 12050; (*b*) A. Stroppa, P. Jain, P. Barone, M. Marsman, J. M. Perez-Mato, A. K. Cheetham, H. W. Kroto and S. Picozzi, *Angew. Chem., Int. Ed.*, 2011, **50**, 5847; (*c*) A. Stroppa, P. Barone, P. Jain, J. M. Perez-Mato and S. Picozzi, *Adv. Mater.*, 2013, **25**, 2284.

30 (*a*) L. Cañadillas-Delgado, O. Fabelo, J. A. Rodríguez-Velamazán, M. Lemée-Cailleau, S. A. Mason, E. Pardo, F. Lloret, J. Zhao, X. Bu, V. Simonet, C. V. Colin and J. Rodríguez-Carvajal, *J. Am. Chem. Soc.*, 2012, **134**, 19772; (*b*) K. S. Hagen, S. G. Naik, B. H. Huynh, A. Masello and G. Christou, *J. Am. Chem. Soc.*, 2009, **131**, 7516; (*c*) J.-P. Zhao, B.-W. Hu, F. Lloret, J. Tao, Q. Yang, X.-F. Zhang and X.-H. Bu, *Inorg. Chem.*, 2010, **49**, 10390.

31 (*a*) P. Jain, N. S. Dalal, B. H. Toby, H. W. Kroto and A. K. Cheetham, *J. Am. Chem. Soc.*, 2008, **130**, 10450; (*b*) T. Asaji and K. Ashitomi, *J. Phys. Chem. C*, 2013, **117**, 10185; (*c*) T. Besara, P. Jain, N. S. Dalal, P. L. Kuhns, A. P. Reyes, H. W. Kroto and A. K. Cheetham, *Proc. Natl. Acad. Sci. U. S. A.*, 2011, **108**, 6828.

32 (*a*) B. Pato-Doldán, M. Sánchez-Andújar, L. C. Gómez-Aguirre, S. Yáñez-Vilar, J. López-Beceiro, C. Gracia-Fernández, A. A. Haghighirad, F. Ritter, S. Castro-García and M. A. Señarís-Rodríguez, *Phys. Chem. Chem. Phys.*, 2012, **14**, 8498; (*b*) A. Rossin, A. Ienco, F. Costantino, T. Montini, B. D. Credico, M. Caporali, L. Gonsalvi, P. Fornasiero and M. Peruzzini, *Cryst. Growth Des.*, 2008, **8**, 3302; (*c*) A. Rossin, M. R. Chierotti, G. Giambastiani, R. Gobettob and M. Peruzzini, *CrystEngComm*, 2012, **14**, 4454.

33 B. Liu, R. Shang, K.-L. Hu, Z.-M. Wang and S. Gao, *Inorg. Chem.*, 2012, **51**, 13363.

34 (*a*) M.-Y. Li, M. Kurmoo, Z. M. Wang and S. Gao, *Chem.–Asian J.*, 2011, **6**, 3084; (*b*) Z. M. Wang, X. Y. Zhang, S. R. Batten, M. Kurmoo and S. Gao, *Inorg. Chem.*, 2007, **46**, 8439.

35 D.-W. Fu, W. Zhang, H.-L. Cai, Y. Zhang, J.-Z. Ge, R.-G. Xiong and S. D. Huang, *J. Am. Chem. Soc.*, 2011, **133**, 12780.

36 (*a*) W. Zhang, H.-Y. Ye, H.-L. Cai, J.-Z. Ge, R.-G. Xiong and S. D. Huang, *J. Am. Chem. Soc.*, 2010, **132**, 7300; (*b*) D. W. Fu, H. L. Cai, Y. M. Liu, Q. Ye, W. Zhang, Y. Zhang, X. Y. Chen, G. Giovannetti, M. Capone, J. Y. Li and R. G. Xiong, *Science*, 2013, **339**, 425; (*c*) H. L. Cai, Y. Zhang, D. W. Fu, W. Zhang, T. Liu, H. Yoshikawa, K. Awaga and R. G. Xiong, *J. Am. Chem. Soc.*, 2012, **134**, 18487.

37 G. Bator, R. Jakubas and L. Sobczyk, in *Crystal Engineering: From molecules and crystals to materials*, ed. D. Braga, F. Grepioni and A. G. Orpen, Kluwer Acad. Pub., Dordrecht, 1999, pp. 459–468.

38 A. B. Cairns and A. L. Goodwin, *Chem. Soc. Rev.*, 2013, **42**, 4881.

39 (*a*) B. V. Nonius, *Collect software*, Delft, The Netherlands, 1998; (*b*) B. V. Nonius, *HKL2000 and maXus softwares*, University of Glasgow, Scotland, UK, Delft, The Netherlands and MacScience Co. Ltd, Yokohama, Japan, 2000.

40 *CrysAlisPro software*, Agilent Technologies UK Ltd, Oxford, UK, 2012.

41 G. M. Sheldrick, *SHELX-97, Program for Crystal Structure Determination*, University of Göttingen, Germany, 1997.

42 L. N. Mulay and E. A. Boudreaux, *Theory and Applications of Molecular Diamagnetism*, John Wiley & Sons Inc., New York, 1976.

43 The Fe products of different batches contained crystals of the two Fe polymorphs, the rectangular pale yellow crystals and the pale blue hexagonal column or bipyramidal crystals. The rectangular crystals have cell dimensions at 290 K as follows: a = 8.7938(3), b = 7.7675(2), c = 11.6312(4) Å, $\alpha = \beta = \gamma = 90°$, V = 794.48(4) Å^3, and the structure was determined. The hexagonal crystals always showed as twinned and we are still trying to determine the structure. However its PXRD (data not given) was very close to that of **3Co**, confirming the existence of the phase.

44 (*a*) D. H. Williams and I. Fleming, *Spectroscopic Method in Organic Chemistry*, McGraw-Hill Book Co, Beijing, China, 5th edn, 1998; (*b*) K. Nakamoto, *Infrared and Raman Spectra of Inorganic and Coordination Compounds*, Wiley, New York, 1986; (*c*) D. Stoilova and V. Koleva, *J. Mol. Struct.*, 2000, **553**, 131; (*d*) D. Stoilova and V. Koleva, *J. Mol. Struct.*, 2001, **560**, 15.

45 M. A. White, in *Crystal Engineering: The Design and Application of Functional Solids*, ed. K. R. Seddon and M. Zaworotko, Kluwer Acad. Pub., Dordrecht, 1999, p. 279.

46 Z.-M. Duan, Z.-M. Wang and S. Gao, *Dalton Trans.*, 2011, **40**, 4465.

47 F. A. Cotton, G. C. Wilkinson, A. Murillo and M. Bochmann, *Advanced Inorganic Chemistry*, Wiley, New York, 6th edn, 1999, p. 1304.

48 A. L. Spek, *PLATON, A Multipurpose Crystallographic Tool*, Utrecht University, Utrecht, The Netherlands, 2001.

49 This was calculated using PCMODEL Version 9.1, see http://www.serenasoft.com

50 Y. Zhang, W. Zhang, S. H. Li, Q. Ye, H. L. Cai, F. Deng, R. G. Xiong and S. P. D. Huang, *J. Am. Chem. Soc.*, 2012, **134**, 11044.

51 K. Aizu, *Phys. Rev.*, 1966, **146**, 423.

52 D. Braga, F. Grepionia and J. J. Novoab, *Chem. Commun.*, 1998, 1595.
53 A. I. Kitaigorodsky, *Molecular Crystals and Molecules*, Academic Press, New York, 1973, p. 18.
54 B. Liu, H.-B. Zheng, Z.-M. Wang and S. Gao, *CrystEngComm*, 2011, **13**, 5285.
55 (*a*) M. Szafrański, A. Katrusiak and G. J. McIntyre, *Cryst. Growth Des.*, 2010, **10**, 4334; (*b*) M. Szafrański and A. Katrusiak, *J. Phys. Chem. B*, 2008, **112**, 6779.
56 (*a*) G. A. Samara, *J. Phys.: Condens. Matter*, 2003, **15**, R367; (*b*) A. A. Bokov and Z.-G. Ye, *J. Mater. Sci.*, 2006, **41**, 31; (*c*) W. J. Kleemann, *Mater. Sci.*, 2006, **41**, 129.
57 A. K. Jonscher, *Dielectric Relaxation in Solids*, Chelsea Dielectrics Press, London, 1983.
58 A. T. Casey and S. Mitra, in *Theory and Application of Molecular Paramagnetism*, ed. L. N. Mulay and E. A. Boudreaux, Wiley, New York, 1976, pp. 183–243.
59 R. L. Carlin, *Magnetochemistry*, Springer-Verlag, Berlin, Heidelberg, 1986, pp. 148–154.
60 J. A. Mydosh, *Spin Glass: an Experimental Introduction*, Taylor & Francis, London-Washington, DC, 1993.
61 M. Balanda, in *Relaxation Phenomena: Liquid Crystals, Magnetic Systems, Polymers, High-TC Superconductors, Metallic Glass*, ed. W. Haase and S. Wróbel, Springer-Verlag, Berlin, Heidelberg, 2003, pp. 97–99.
62 (*a*) M. Mito, K. Iriguchi, H. Deguchi, J. Kishine, K. Kikuchi, H. Ohsumi, Y. Yoshida and K. Inoue, *Phys. Rev. B: Condens. Matter*, 2009, **79**, 012406; (*b*) M. Mito, K. Iriguchi, H. Deguchi, J. Kishine, Y. Yoshida and K. Inoue, *J. Appl. Phys.*, 2012, **111**, 103914.
63 (*a*) I. Dzyaloshinsky, *J. Phys. Chem. Solids*, 1958, **4**, 241; (*b*) T. Moriya, *Phys. Rev.*, 1960, **120**, 91; (*c*) T. Moriya, in *Magnetism*, ed. G. T. Rado and H. Suhl, Academic Press, New York, 1963, vol. 1, pp. 85–124.

